This is to certify that the
thesis entitled

GEOCHEMISTRY OF THE UPPER DILIMAN TUFF UNIT IN MANILA, SOUTHWEST LUZON, PHILIPPINES: INSIGHTS ON ITS ORIGIN AND COMPARISON WITH TAAL AND LAGUNA CALDERA PYROCLASTIC FLOWS

presented by

MARIA CARMENCITA B. ARPA

has been accepted towards fulfillment
of the requirements for the

M.S. degree in GEOLOGY

Major Professor's Signature

5-19-05

Date

GEOCHEMISTRY OF THE UPPER DILIMAN TUFF UNIT IN MANILA, SOUTHWEST LUZON, PHILIPPINES: INSIGHTS ON ITS ORIGIN AND COMPARISON WITH TAAL AND LAGUNA CALDERA PYROCLASTIC FLOWS

By

Maria Carmencita B. Arpa

A THESIS

Submitted to
Michigan State University
in partial fulfillment of the requirements
for the degree of

MASTER OF SCIENCE

Department of Geological Sciences

2005

ABSTRACT

GEOCHEMISTRY OF THE UPPER DILIMAN TUFF UNIT IN MANILA, SOUTHWEST LUZON, PHILIPPINES: INSIGHTS ON ITS ORIGIN AND COMPARISON WITH TAAL AND LAGUNA CALDERA PYROCLASTIC FLOWS

By

Maria Carmencita B. Arpa

The upper Diliman Tuff is a basaltic to dacitic pyroclastic flow, which overlies the sequence of tuffaceous deposits found north of the southwest Luzon volcanic field in the vicinity of Manila, Philippines. Pumice fragments from this deposit are high-K basalt to dacite (50–65 wt. % SiO_2). These pumices are glassy with 1–3 % phenocrysts content, mainly plagioclase and pyroxene. Mingling textures occur and there is variability in glass compositions for a single pumice. Disequilibrium features are also seen in the phenocrysts. Bulk trace element composition and mineral chemistry indicate mingling of magmas. The chemical variation in the deposit can be explained by mixing of melts produced by different degrees of partial melting. Volcanism in Luzon is produced largely from subduction and in the southwestern portion, extension. During subduction, the overriding crust is modified by emplacement of subduction-related magmas and partially melted by hot basaltic intrusions generated in the mantle wedge beneath southwest Luzon. The location of the actual vent or source volcano of the upper Diliman Tuff deposit is uncertain; comparisons show that it is chemically distinct with respect to deposits from adjacent Taal and Laguna calderas. Differences with these volcanic centers are seen in terms of major and trace element compositions.

ACKNOWLEDGEMENT

It was lucky for me that Tom Vogel, Lina Patino and Tim Flood did fieldwork in the Philippines. I thank Tom for helping me collect my samples. I'd also like to thank my adviser, Lina Patino for all her help, guidance and patience. I'm thankful for having Tom Vogel and Kaz Fujita in my committee. Taking their classes also, has been very informative for me and important in making me understand my research. I appreciate all the classes I took here at MSU. I also learned a lot from classmates and meetings of the petrology group – Dave, Karen, Beth, Chad and Ryan.

I thank PHIVOLCS for the work experience and maturity: RSP for encouraging and inspiring us; Rene Solidum for letting me study the cores; Remon, Mabel, Toto, Mylene, Hannah and Peejay for their help; Norman for being a cool boss.

I thank my friends for keeping me sane: friends from Owen Hall - Ma-an, Gizelle, Andrew, Nate, Tim and Stacy.

I thank Jérôme for encouraging me and for being the best part of my stay here.

Finally, I thank my father, my mother, my sister Tet and my niece Amber for their support and most of all, example.

TABLE OF CONTENTS

LIST OF TABLES

LIST OF FIGURES

Formatting note

Images in this thesis are presented in color

Introduction

There are several layers of pyroclastic deposits (Diliman Tuff) found in the Manila area, Southwest Luzon, Philippines. This study will focus on the uppermost unit (upper Diliman Tuff), which has pumice fragment compositions that range from basalt to dacite. Although the volcanic source of this deposit is unknown, there are several possible sources: the nearest volcanoes to the north and northwest and to the south and southeast.

The first objective of this study is to chemically characterize the upper Diliman Tuff and to compare it with deposits from known sources in the vicinity. Two possible source volcanoes were chosen for comparison. One is Laguna caldera which is 40 km to the southeast; it is the nearest volcanic center to the deposits. The other is Taal caldera, 60 km to the south. The youngest deposit from Taal caldera, a scoria pyroclastic flow dated 5,000 years B.P., is found just south of Manila (Martinez, 1997). Older deposits of Taal caldera have more silicic compositions (Listanco, 1993). Laguna caldera also has several units of pyroclastic flow deposits, but the stratigraphy is less constrained than Taal (Catane et al., 1998, unpublished report). Comparison, therefore, will be done to a range of deposits from Taal caldera, including Volcano Island, and Laguna caldera.

The second objective is to determine possible processes that produced the range in SiO_2 content of the pumice fragments in the unit. Possible processes that can produce silicic rocks are fractional crystallization, partial meting of crustal rocks and assimilation. In evaluating the processes, the conditions set from the geologic setting must be considered. Presently, volcanism in west Luzon is due to the subduction of the South China Sea Plate along the Manila Trench. Knittel and Defant (1988) suggested that prior

to subduction in the Manila Trench, the Philippine arc evolved from a mantle source more enriched than a MORB source. This conclusion is based on isotopic compositions of pre-Manila Trench subduction-related intrusives in Luzon and the modern arc. Since subduction began in the Manila Trench, source materials for some volcanoes in Luzon have been more enriched in Large Ion Lithophile Elements (LILE) and radiogenic Sr as a result of dehydration of the subducted crust and terrigenous sediments from Eurasia (Knittel et al., 1988, Defant et al., 1988, Mukasa et al., 1994, Castillo and Newhall, 2004).

In this study, major and trace element compositions of pumices and their component minerals shall be used to correlate to a source volcano, and to understand the origin and evolution of the magma that produced the deposits. Data include XRF and LA-ICP-MS analyses of individual pumice fragments. Microprobe analyses of the mafic and felsic glass in the mixed pumices and individual minerals will test the relationship of the magmas with respect to each other. Mineral chemistry will give estimates of pressure and temperature conditions during crystallization, which will have implications on the depth of the reservoir.

Geologic setting of Southwest Luzon

Manila is located north of the southwest Luzon volcanic field where both Laguna and Taal calderas are found. The southwest Luzon volcanic field is a region consisting of strato-volcanoes, monogenetic centers and calderas (Oles et al., 1995). Volcanoes in southwest Luzon can be related to eastward directed subduction in the Manila Trench and extension in the Macolod Corridor (Knittel et al., 1988; Defant et al., 1988; Forster et al., 1990) (Figure 1a-b).

The Philippine arc, which includes most of Luzon Island, probably developed on Philippine Sea basaltic crust. It was part of the Philippine Sea Plate before the development of the Philippine mobile belt, which is marked by subduction zones to the east and west (Rangin et al., 1995). Subduction along the west margin, offshore of Luzon, is along the Manila Trench. The eastward subduction of the South China Sea Plate in the Manila Trench started between Late Oligocene to Middle Miocene (Hayes and Lewis, 1984). The South China Sea opened in the Middle Oligocene/Early Middle Miocene, around 32-15 Ma B.P. (Taylor and Hayes, 1983; Pautot and Rangin, 1989). Manila Trench extends from 13° to 20° N, trends North-South, and is almost linear instead of arcuate due to the indentation caused by the subduction of the axial ridge of the South China Sea offshore of Central Luzon (Hayes and Lewis, 1984; Pautot and Rangin, 1989). The dip of the subducting slab also changes from North to South along the trench and becomes almost vertical towards the southern end (Cardwell et al., 1980). Volcanism in Southwest Luzon from this subduction occurs around 100 to 200 km above the Wadati-Benioff zone (Cardwell et al., 1980). The area where the dip of the subducting slab is almost vertical is marked by the Palawan-Mindoro collision, which involves the

North Palawan Continental Terrane (Figure 1a) (Cardwell et al., 1980; McCabe et al., 1985). It was suggested that slivers of this continental terrane could have been assimilated by the magmas of some southern Luzon volcanoes (Knittel and Defant, 1988). Seismic refraction and reflection sections taken offshore of Central Luzon (15.5° N) show that the Manila Trench has a well developed accretionary prism and that hemipelagic sediments are subducted and not scrapped off with the turbidites (Hayes and Lewis, 1984). This information is important in evaluating magmatism related to subduction where dehydration, and probably melting of the sediments, are envisioned (Castillo and Newhall, 2004).

In southwest Luzon, there are volcanoes located east of the west-facing volcanic arc that are not above a subducted slab. These structures and volcanoes, dated 6 Ma to present (Oles, et al., 1995), defined the Macolod Corridor (Figure. 1b.), which is a NE-SW trending rift zone crossing the Philippine arc in SW Luzon (Defant et al., 1988, Forster et al., 1990). The direction of extension in the corridor was suggested to have changed from N-S and NNW to NW and finally to E-W rifting (Pubellier et al., 2000). Volcanism from 2 Ma to present may be related to the E-W extension. The present E-W extensional direction could be a reaction to the collision of the Palawan block with the Philippine arc (Pubellier at al., 2000). This collision began around 10 Ma (Rangin et al., 1995). Generally there is a counter-clockwise rotation of Luzon above this collision reflected by the higher rate of convergence in the northern part of Manila Trench as compared to the south (Pubellier et al., 2000). More recent studies involving GPS modeling show left-lateral transtensional movement in the Macolod Corridor at a rate of 11-13 mm/yr. (Galgana et al., 2004).

There is also another subduction on the east side of the Philippines (Figure. 1a) but it may not be related to the present volcanism in SW Luzon or the past activities of Laguna or Taal calderas. The west-facing subduction in the Philippine Trench is a younger feature and the slab does not reach below SW Luzon (Cardwell et al., 1980). Volcanic centers related to subduction in the Philippine Trench are located in the Bicol arc farther to the southeast.

Taal Caldera

Taal caldera is located just slightly east of the Bataan arc, which forms the trench-side volcanic chain for the subduction in the Manila trench (Figure. 1b). The depth of the slab beneath Taal is estimated to be 200 km (Cardwell et al., 1980). Caldera formation stage was from 140,000 to 5,380 years ago and produced calc-alkaline andesitic to dacitic ignimbrite eruptions (Listanco, 1993). The youngest caldera eruption is basaltic and occurred around 5,000 years B.P. (Martinez, 1997). Composition of Taal lavas are significantly influenced by subducted terrigenous sediments of the South China Sea basin (Miklius et al., 1991; Castillo and Newhall, 2004). Based on fractional crystallization modeling, the silica variation for Taal lavas is due to mixing of melts from separately evolving fractionation systems supplied by melts from a heterogenous mantle source (Miklius et al., 1991).

Laguna Caldera

Laguna caldera is located around 30 km east of Taal (Figure. 1b). The caldera is difficult to outline but it is generally in Laguna de Bay lake. Laguna de Bay is a horst

and graben feature composed of N-S trending structures that have been modified by volcanism. The caldera outline proposed by Wolfe and Self (1983) coincides with the middle lobe of Laguna de Bay. The Laguna Tuffs include flat-lying volcanics, flows, tuffs, and coarse agglomerates (Corby, 1951). Welded ignimbrites are extensive around the caldera margin. The episode of magmatism attributed to Laguna caldera occurred between 2.3 to 0.9 Ma based on K-Ar dates in andesitic and rhyolitic lava and tuff deposits (Oles et al., 1995). Radiocarbon dating of a pyroclastic flow deposit gives an age of around 47,000 B.P. (Catane et al., 1998, unpublished report). Deposits from Laguna contain pumice fragments compositions between 53 to 69 wt. % SiO_2 (Flood et al., 2004). Flood et al. (2004) suggested that the high silica magmas of Laguna were generated by partial melting or assimilation of previously emplaced calc-alkaline material based on high Na_2O/K_2O ratios.

General geology of Manila

The Metro Manila (MM) region can be physiographically divided from west to east into the coastal region, Quezon City plateau, Marikina valley, and the Antipolo Highlands (Figure 2). Recent alluvial deposits overlie the Marikina valley and coastal regions. Underlying pyroclastic deposits are well exposed in the Quezon City plateau. Pyroclastic deposits from Taal caldera cover the southernmost part of MM (Martinez, 1997). The Antipolo Highland is the southern extension of the Sierra Madre Range and is composed partly of old volcanics and sedimentary rocks that are included in an ophiolite suite (Arcilla, 1991). Marikina valley and Quezon City plateau are a graben and horst produced by movements along the Valley Fault (Marikina Fault) (Alvir, 1929;

Gervasio, 1968). The Marikina valley extends southward into the western lobe of Laguna de Bay.

Pyroclastic deposits in Manila

The pyroclastic deposits found in Manila belong to the Guadalupe Tuff formation. This formation is characterized as consisting of angular chunks of volcanic debris with a thickness that may vary from 1,300 to 2,000 meters (Corby, 1951). The type section is at Guadalupe in Manila along the Pasig river. Corby (1951) mentioned that these are probably fine grained facies of the Laguna Tuff farther east. The Laguna Tuffs however were still assigned as a separate formation and only includes the volcanics in the vicinity of Laguna de Bay (Corby, 1951). Another study divided the Guadalupe Tuff into two members, namely Alat conglomerate and Diliman Tuff (Teves and Gonzales, 1950). Diliman Tuff is the tuff sequence in the formation with the type section in the Diliman area in Quezon City. The Diliman Tuff consists of flat-lying beds of fine-grained, vitric tuffs and welded volcanic breccias with minor amounts of tuffaceous sandstones (Gonzales et al., 1971). An 18 to 21 m exposure in Guadalupe shows an upper stratigraphic section of the tuffs that include three horizons of erosional surfaces marked by fossil soil or decayed tuff (Gervasio, 1968).

This study focuses only on the upper unit of the Diliman Tuff. Data for this unit are gathered from short cores (10 m), long core (40 m) and outcrops. The short cores intersected only one set of pyroclastic flow deposits. In all the short cores, two types of pyroclastic deposits were identified. One group of correlated cores, which includes borehole 7 (BH07), shows a pyroclastic flow deposit that contains coarse lapilli size pumice, scoria (mafic pumice) and banded pumice. Below this pyroclastic flow unit are finer grained layers interpreted as surge and fall deposits. The second group, which is not part of this study, can be seen in borehole 15. BH-15 recovered thick tuffs (mostly fine ash) rich in accretionary lapilli and interbedded with ash layers containing lapilli-sized pumice and scoria. These are interpreted as pyroclastic surge and fall deposits. Associated with the deposits in BH-15 are unwelded and fine grained pyroclastic flows that are either pumice-rich or scoria-rich. Outcrop exposures where samples were taken are at sites 040303-1 (Quezon City), 040303-2 (Pasig) and 040303-3 (Pasig) (Figure. 3b-d). The pyroclastic flow deposit at site 040303-1 is lithic-rich and slightly weathered with a soily matrix. Pumice samples from this unit are colored black and brown, and some are banded. The pyroclastic flow deposit at 040303-2 is 7 m thick and is composed of coarse lapilli-sized mafic pumice and finer, lighter pumice and banded pumice clasts. At site 040303-3, the pyroclastic flow unit is around 10 m thick and overlies paleosol/weathered ash and a tuffaceous fluvial deposit. It consists of mostly light brown to white pumice clasts. Correlation of outcrops and core samples gives a stratigraphic sequence consisting of (from top to bottom): a) a coarse grained pyroclastic flow deposit with black to light gray/white pumice clasts; b) a weathered ash (possibly a soil); c) a thick sequence of fines-rich surge and fall deposits; and d) another coarse grained pyroclastic flow deposit (Figure 4).

Methods

A total of 23 pumice fragments from 3 outcrops of a pyroclastic flow deposit in Metro Manila were sampled (Table 1). Additional samples were collected from borehole cores archived by the Philippine Institute of Volcanology and Seismology (PHIVOLCS). Pumice fragments (18) were picked from cores, which sampled the pyroclastic flow unit for this study. The small size of some pumice clasts limits the sampling. For the analytical methods that were applied, a minimum of 1.0 gram of dry sample is required. The pumice clasts are within the lapilli size range (2-64 mm) (figures 5 and 6). Pumice fragment variety based on color (light, dark and banded) was considered in sampling. For the comparison study, pumice fragments from several pyroclastic flow units from Laguna caldera were also collected.

Pumice samples from the Diliman Tuff unit were all hand ground using an opal mortar and pestle. Smaller samples from Laguna units were hand ground and the rest were powdered using an aluminum flat plate grinder after passing through a chipmunk. There are two recipes for the fused glass disks: the Low Dilution Fusion (LDF) and High Dilution Fusion (HDF). The standard is the LDF. For smaller samples, the HDF had to be used. In the LDF, 3.0000 +/- 0.0005 grams (g) of finely ground pumice powder were diluted by adding 9.0000 +/- 0.0005 g lithium tetraborate ($Li_2B_4O_7$) flux and 0.5 g ammonium nitrate (NH_4NO_3) as an oxidizer. For the HDF, only 1.0000 +/- 0.0005 g of pumice powder is mixed with the same amount of flux and 0.16 g oxidizer. Fifteen HDF disk were made and the rest of the samples were fused into LDF disks. For a sample weighing ≥1.500 g, half of the proportions in the LDF recipe were used making smaller disks. The dry mixed powder was melted in platinum crucibles at 1000°C of oxidizing

flame for >20 minutes while being stirred with an orbital mixing stage. Platinum molds were used to make the glass disk.

Analysis for major and trace element were done using a Rigaku S/Max X-ray Fluorescence Spectrometry (XRF) and additional trace element and rare-earth element analysis by Laser Ablation Inductively Coupled Plasma Mass Spectrometer (LA ICP-MS) at Michigan State University. Major element data from the XRF were calculated using fundamental parameters and trace elements were calculated using a linear regression. For LA ICP-MS analyses, strontium determined by XRF was used as an internal standard. Element concentration was based on linear regression method using BHVO-1, W-2, JB-1, JB-2, JB-3, JA-2, and BIR standards. The same glass disks were used for both XRF and LA ICP-MS.

Electron microprobe analysis was done at the Department of Geological Sciences, University of Michigan using an SX 100 CAMICA microprobe. A beam size of 5 microns at a beam current of 10 nA was set for the mineral analyses. Plagioclase and pyroxene compositions were analyzed in seven pumice clasts, and glass compositions were determined in nine pumice fragments.

Petrography

The pumice clasts in the upper Diliman Tuff are varied in terms of color and texture. Mafic, felsic and banded pumice fragments are present and there is a range in the degree of vesiculation. Generally, the pumices are glassy and finely vesiculated. Sample PIVS1-9.28A contains non-vesiculated black bands. The phenocrysts make up only 1 to 3 % of the bulk. Sometimes they occur as glomerocrysts. Coarse phenocrysts are around 1 to 2.5 mm for the longest side but usually the crystals are smaller. The mineral phases are plagioclase, clinopyroxene, orthopyroxene and magnetite. Magnetite is sometimes included in pyroxene and plagioclase. Amphibole and mica are found only in the most silicic samples. Trace phases are apatite and zircon. Mingled pumice clasts show banding of light and dark glass. Even pumice fragments that do not show obvious mingling in hand sample may show mingling microscopically. Some pumice fragments contain enclaves.

Groundmass

The groundmass is mostly glass. It is brown to dark brown in the most mafic pumice samples and clear glass in the higher silica pumice samples. The dark color can also be due to oxide crystallites in the glass, but the oxide specks are most common in the mafic pumices. Sometimes dark brown to black bands are present (040303-1M) and the groundmass appears mottled. In sample 040303-1C, which is a banded pumice, groundmass is light to dark brown glass (Figure. 7).

Plagioclase

Plagioclase crystals are the most abundant phase and are commonly fractured. Crystals are typically euhedral to subhedral and some with rounded edges (Figure 8). Sieved texture and glass inclusions are present and for some, only at concentric zones or at the core. Zoned crystals are present which can show distinct zones or irregular boundaries. Normal, reverse and oscillatory zoning occurs. The coarsest plagioclase lath is 1.7 mm^2.

Pyroxene

The second most abundant phase is pyroxene (Figure 9). Both clinopyroxene and orthopyroxene are present. Some show slight resorption and few are zoned. The coarsest pyroxene crystal is 1.6 mm^2.

Enclaves

Enclaves are present in samples PIVS1-9.28A and BH07-01-S1. There are three kinds of enclaves found in PIVS1-9.28A based on texture. The first (Figure 10) is microlitic with glomerocrysts of plagioclase. It is composed mostly of plagioclase with some clinopyroxene. The plagioclase glomerocrysts are zoned, with corroded edges and are sieved. The second (Figure 11a) consists of acicular plagioclase crystallites with one larger plagioclase lath. It is almost cryptocrystalline. The third (Figure 11b) is porphyritic with around 40% phenocrysts--mostly plagioclases that are zoned and resorbed and few smaller clinopyroxenes. In sample BH07-01-S1, the enclave is non-vesiculated, black and banded with trace plagioclase crystallites.

Geochemistry

Whole rock geochemistry

The samples were prepared differently, mostly by LDF but some by HDF, due to limitations in the amount of sample. Detection limits in HDF samples are poor for trace elements. The 10 samples prepared by HDF will be excluded in the trace element plots. Samples with less than 95 wt. % total are considered altered and were excluded from the data set (Table 2). All oxide values were normalized to 100 % for plotting.

Major element compositions

The pumice clasts for the upper Diliman Tuff unit have SiO_2 compositions ranging from basalt to dacite (50–65 wt. % SiO_2) (Figure 12) with the andesitic to dacitic compositions being in the high-K range (Figure 13). Major element variations with silica show increasing K_2O (1-4 wt.%) and Na_2O and a decreasing trend for the other major elements (figure 13). The samples also have high FeO values (5-11 wt.%) compared with average island arc volcanics (0.5-7.4 wt. %) (Winter, 2001), and decrease at a greater rate compared with MgO. It should be noted that two samples (040303-1I and 040303-1F) have lower MgO value and do not plot on the general MgO trend. Some samples (040303-1A, B, E, F, G, H, I, K, M) have unusually high P_2O_5 concentrations (1.14 to 2.78 wt. %). The average value for P_2O_5 in island arc volcanics is 0.1 to 0.5 (Winter, 2001).

The most basaltic samples (040303-1A, B, E, F, G, H, I, K, M), with the exception of PIVS1-9.28A, have the lowest total alkalis values and plot in the tholeiitic field (Figure 14). In a plot of total alkalis versus Mg# (Figure 15), they have a separate

trend to the rest of the samples. The basaltic andesite to dacite samples have high total alkalis values compared to the previous group. These samples plot in the lower basaltic trachyandesite to trachydacite field. The lowest silica samples in this set are PIVS1-9.28A, PIVS1-9.48A, PIVS1-10.97A (open triangles) (Figure 12).

Trace element compositions

Spider diagrams for the upper Diliman Tuff pumices show a typical island arc pattern (Figure 16), having pronounced depletion in Nb and Ti and enrichment in LIL elements. Two patterns were recognized. The first is for the mafic group with high P_2O_5 (Figure 16a) mentioned in the major element section. The pattern for this group shows distinctive positive spikes for U, La, Pb and P. It also has lower concentrations for LILE, such as Rb, Ba, K, and Pb compared to the higher SiO_2 pumices. On the otherhand, the spidergram for the second group of pumices (Figure 16b) (53 to 65 wt % SiO_2) shows an overall decreasing trend from incompatible to compatible elements, with obvious positive spike for Pb and depletion in Nb and Ti.

Trace element variations with silica (Figure 17) are plotted to show trends in concentrations and influences in later element ratio plots. Values for Sr decrease, while Rb increase, with increasing silica. HFS (High Field Strength) elements such as Nb, Th and Zr increase slightly with increasing SiO_2. A steep negative slope can be seen for V. For Yb and Lu, one trend has consistently higher concentrations for the same values of silica.

Chondrite-normalized REE distribution shows a tight pattern for a silica range of 50 to 64 wt. % (Figure 18). The pattern displays enrichment in light REE (LREE)

relative to heavy REE (HREE) with concentration values typical for representative high-K basaltic andesites and andesites. The Eu anomaly is very small and there is only a very slight depletion in the middle heavy REE.

Mineral chemistry

Plagioclase

Plagioclase compositions range from An_{36} to An_{90} (Table 3). Crystals show the normal increase in An content with decrease in bulk SiO_2 content of the pumice clasts (Figure 19). As mentioned, the plagioclases are zoned. Maximum difference between core and rim is 12% An. Both normal and reverse zoning are present. In a zoned plagioclase in sample 040303-3B (whole rock=63.33 wt.% SiO_2) core to rim An content goes from 61 to 50% An. Sample 040303-1N (whole rock=56.1 wt.% SiO_2) contains a plagioclase with oscillatory zoning that goes from 73 to 81 to 79% An. A reverse zoned plagioclase in sample PIVS1-9.28A (whole rock=52.62 wt.% SiO_2) has 67% An in the core and 80% An in the rim (Figure 20).

As mentioned, there are 3 types of enclaves in sample PIVS1-9.28A initially based on texture (see petrography section). Plagioclase chemistry in each enclave turned out to be distinct (Figure 20). Enclave 1 has plagioclase with An content ranging from 52% to 68%. A large zoned plagioclase phenocryst (pl1) has reverse zoning from An_{58} (core) to An_{68} (rim). Groundmass plagioclases (pl2 to pl4) have An_{52} to An_{67}. In enclave 2, there is only one plagioclase (An_{49}) large enough to be analyzed. The plagioclases in enclave 3 have the highest Anorthite content (An_{76} to An_{93}).

Pyroxene

Two types of pyroxenes are found in the pumice samples (Figure 21): clinopyroxene with $Wo_{38}En_{46}Fs_{15}$ to $Wo_{45}En_{41}Fs_{14}$ and orthopyroxene with $Wo_3En_{66}Fs_{30}$ to $Wo_4En_{70}Fs_{26}$ (Table 3). Both clinopyroxene and orthopyroxene are found in pumice samples with bulk SiO_2 of 61.23 to 63.33 wt. %. Only clinopyroxene is found in the lower silica pumice samples. In the enclaves, both enclave 1 and enclave 3 have clinopyroxene ($Wo_{36}En_{45}Fs_{20}$ to $Wo_{40}En_{42}Fs_{18}$). Mg # for the pyroxenes range from 53 to 64. Two groups are also identified using Al/Ti ratio (Figure 22). The group with a lower ratio includes all the orthopyroxenes and most of the clinopyroxenes. The group with a higher ratio includes all clinopyroxenes in enclave 1 and a clinopyroxene in its host pumice, PIVS1-9.28A.

Glass Chemistry

Glass compositions range from 54.32 to 66.04 wt. % SiO_2 for the 9 pumice samples analyzed (Table 3). Bulk SiO_2 is plotted with glass SiO_2 to show that glass composition is variable for individual pumices (Figure 23). A significant range is seen in samples BH07-03-P3, 040303-1C, 040303-2C, and BH07-03-C (54.32 to 65.28 wt. %). Pumice PIVS1-9.28A, which is basaltic with anorthitic plagioclases, has 64.55 to 66.04 wt. % SiO_2 glass. Glass compositions in the enclaves are also analyzed (Table 3). In the MgO versus SiO_2 diagram, enclaves 2 and 3 plot below the trend (Figure 23).

Discussion

Evaluation of crystal fractionation

Although fractional crystallization is consistent with some element variation trends with silica (Figure 17), other parameters are inconsistent with fractional crystallization. For the majority of the samples, there is no clear fractionation trend that goes from more primitive to more evolved as seen from the plot of Mg# versus SiO_2 (Figure 24). In addition, the REE patterns have a narrow distribution for the entire range of silica composition (Figure 18). This can also be seen in the REE variation with increasing silica where the REE concentrations increase only slightly or are almost constant. Note also that for the HREE, there are two concentration trends for the same value of SiO_2 (Figure 17). Fractional crystallization, provided there is no large fractionation of pyroxenes and garnets, would produce parallel and increasing concentration REE patterns as silica increases, which is not the case for the upper Diliman Tuff pumice fragments. Certain groups, such as the most basaltic samples that plot in the tholeiitic field, have trends that probably reflect slight olivine fractionation. Relative to the rest of the samples with higher total alkalis, this group (i.e., tholeiitic) shows more pronounced decrease in Mg# (Figure 15). The samples with higher total alkalis, although with silica values from 53 to 64 wt. %, have a narrow Mg# range, which could reflect suppression of olivine crystallization by addition of an alkali-rich silicic component (Dungan, 2005). Two populations can be seen in the plot of FeO/MgO versus SiO_2 for the glass and bulk compositions (Figure 25). In the bulk compositions, samples 040303-1I and F have the higher FeO/MgO ratio (Figure 25a). Glass in enclaves 2 and 3 have higher FeO/MgO (Figure 25b). This group (enclave 2 and 3 and pumice samples)

probably represents a basaltic intrusion where again there were some fractionation of olivine, since the reason for the high ratio is low values for MgO.

Evidence of magma mingling

The pyroclastic flow deposit in this study consists of a mixture of pumices with a range of compositions. Mingling within pumice fragments, disequilibrium textures in the crystals, and heterogeneity in the glass compositions are interpreted as evidence for the mingling or mixing of magmas. Disequilibrium features in the minerals such as zoning may indicate mixing/mingling of different composition liquids. To illustrate this, the composition of plagioclases for rim and core in pumice and enclaves are shown in separate graphs (Figure 20). When a mafic melt is introduced into a magma body, reverse zoning is observed while normal zoning can reflect fractional crystallization or mixing with a more silicic melt. Enclave 3 has the most anorthitic plagioclase core with the rims less anothitic. Enclave 1 has plagioclases (the core of a zoned phenocryst and groundmass plagioclases) with similar anorthite content to the plagioclases in higher silica pumice samples (>60 wt. %). For the zoned plagioclase in enclave 1, the rim has higher anorthite. Reversely zoned plagioclases in the host pumice PIVS1-9.28A have core compositions similar to either plagioclase rim composition of enclave 1 or plagioclase compositions in enclave 3.

The chemistry and texture of the glass in the pumices clearly shows mingling. A mixing line can be fitted in the data set (Figure 26). The fit depends on the end points chosen. Samples BH07-03-C-gm4 (54.32 wt.% SiO_2) and PIVS1-9.28A-gm1 (65.05 wt. % SiO_2) as end points covers the entire range of compositions though the fit is slightly

offset. Glass analyses from enclave 2 and 3 do not fit in this line whereas enclave 1 glass fits with the trend. A mixing line can also be fitted through the bulk pumice compositions (Figure 27). In this diagram, samples that plot in the tholeiitic field (040303-1) deviate from the trend, and this is more pronounced in samples 040303-1I and F.

Evaluation of partial melting

La/Yb ratio can be used to show relative degrees of partial melting. La/Yb values for all the pumice samples from the upper Diliman Tuff have a range of around 6.5 to 11.5. The distribution is such that basaltic samples with 50-57 wt.% SiO_2 have values of 7.5 to 11.5; andesitic samples (whole rock=58–62 wt.% SiO_2) have around 6.5 to 11; and samples with SiO_2 wt. % of 63 to 65 have ratios from 6.5 to 10 (Figure 28a). From this, it appears that there is no pattern for La/Yb ratio with increasing differentiation. However, this variation could represent different batches of melts. The higher silica samples are not related to the low silica samples by fractional melting based on La/Yb ratio since the low silica samples have the higher ratio. The higher silica (andesitic to dacitic) samples were produced by higher degrees of partial melting compared to the basaltic samples. Furthermore, there appears to be two batches of basaltic melts: one have the highest La/Yb ratio in the data set and the other has lower ratios and consists of the tholeiitic samples (Figure 28). The first group of basaltic samples mentioned has high alkali content, consistent with low degree partial melting. The partial melts produced could mix or mingle. Mingling was already discussed in the previous section, and the chemical variations in the samples can be interpreted as a result of mingling of different

melts. The enclaves could represent remnants of earlier crystallized magmas that were partially melted by a new intrusion or mafic magma that was intruded into another. Adding more heterogeneity, some of these intrusions are tholeiitic and some are calc-alkaline, as shown from major element compositions.

Pressure and temperature estimates

Mineral compositions can be used to determine the temperature and pressure of crystallization. Total Al/Ti in clinopyroxene can be correlated to the crystallization pressure (Figure 22) (Thompson, 1974; Pilet et al., 2002). Based on Ti and Al compositions, it can be interpreted that clinopyroxenes in enclave 1 crystallized in a higher pressure regime. Al/Ti ratios in clinopyroxene and plagioclase compositions imply a batch of magma at lower pressure and temperature, and melts coming from higher temperature and pressure. To estimate temperatures of crystallization, geothermometry was done for pumice samples containing both orthopyroxene and clinopyroxene, using the software QUILF (Andersen et al., 1993) (Figure 29). Temperature estimates for samples 040303-3B and 040303-2C have lower uncertainty due to additional constraint from magnetite. The temperature estimated is around 850°C. This temperature is for the magma from shallower levels. The samples from which this temperature is estimated have the two types of pyroxenes and lower Al/Ti ratio for the clinopyroxene crystals. Clinopyroxene with higher Al/Ti ratio and the most calcic plagioclase crystals are also found in the host pumice PIVS1-9.28A. The presence of these crystals in this sample could mean that the host magma crystallized to some extent at higher pressure or that the minerals are disaggregated grains from the enclaves.

Source comparison with Taal and Laguna Caldera

The source of the upper Diliman Tuff is unknown. Comparison with the nearest vents for large-scale eruptions of pyroclastic deposits, Taal Caldera and Laguna Caldera, shows that the deposits are different. Figure 30 shows selected major and trace element variation with silica for the upper Diliman Tuff unit, Taal (Martinez, 1997, Listanco 1993, Miklius et al., 1991) and Laguna deposits (MSU data). The Manila deposits have higher K_2O, Sr and Rb values as compared to Taal, and clearly, these cannot be correlated. The trends for the upper Diliman Tuff are closer to Laguna pyroclastics. However, differences can be seen, particularly in the low silica compositions in the TiO_2 and MgO variation diagrams (Figure 30). Figure 31 includes samples with SiO_2 values from 53 to 67 wt. % and shows that Manila samples are more primitive and have higher Mg#, than Laguna samples for the same range of total alkalis. Nonetheless, spider diagrams show little differences between Manila and Laguna pyroclastic flow deposits (Figure 32). The REE pattern is also similar except for basaltic pumices. REE diagrams for the deposits (Figure 33) show higher concentrations for the more basaltic pumice of the upper Diliman Tuff compared with Laguna even though the samples for Laguna are less basaltic (SiO_2 values ranging from 53 to 67 wt. % compared with Manila's SiO_2 values from 50 to 65 wt. %). As a result, Laguna deposits have a wider range of REE concentrations than the pattern shown by the deposits in Manila. The similarities in trace element concentrations and differences in major elements for the upper Diliman Tuff and Laguna pyroclastic flows can be interpreted as a difference in source but with similarities in differentiation processes.

Comparing the La/Yb ratios of the upper Diliman Tuff with Taal and Laguna exclusively using the samples with SiO_2 range of 56–60 wt.%, it appears that ratios increase with increasing distance from the trench (Figure 28b). Taal deposits have La/Yb ratios that range from 6 to 8 and Laguna deposits have ratios from 8.5 to 12. The wide range of values for the deposits from Manila is intermediate between Laguna and Taal.

Model for the origin and evolution of the upper Diliman Tuff

There are several models to explain the compositional variation, particularly production of silicic magmas, in island arcs. Felsic volcanism in oceanic volcanic arcs, such as the Kermadec arc, can be explained by dehydration melting of underplated arc material (Smith et al., 2003). Silicic melts in the Costa Rican arc have been explained by partial melting of relatively hot subduction related magmas that have ponded in the crust (Hannah et al., 2002; Vogel et al., 2004). Models of melting caused by intrusion of hot basalt into the deep crust show that a wide range of melt compositions can be produced simultaneously (Annen and Sparks, 2002). Partial melting of the crust is caused by heat transfer from the crystallizing basalt intrusions (Annen and Sparks, 2002; Vogel et al., 2004). Generated melts in the crust and residual melt from the crystallizing basalt can mix/mingle and end up in the same erupted deposit (Annen and Sparks, 2002).

The basaltic intrusions originate from the mantle. Water released from down-dragged hydrated mantle peridotite or subducted lithosphere causes partial melting of overlying mantle wedge peridotites (Tatsumi, 1989; Grove et al., 2003). In subduction zones, most of the water introduced into the system comes from the hydrated subducting crust and sediments (Tatsumi, 1989; Peacock, 1990; Giggenbach, 1992).

The model proposed here for the generation of magma that was erupted as the upper Diliman Tuff is partial melting of the overriding crust by hot basaltic intrusions originating from a metasomatised mantle wedge. Figure 34 and 35 illustrate the processes involved. Sources for Luzon volcanoes are typical for subduction zones where there is enrichment in LILE carried by aqueaous fluids from the subducted slab (Knittel et al., 1988, Defant et al., 1988, Mukasa et al., 1994). Generally, the amount of fluids released during subduction decreases with depth, but a series of hydration and dehydration reactions as depth increases brings fluids to deeper levels. At pressures greater than 3.5 GPa, the stable hydrous phases are Phlogopite and K-amphibole. Dehydration of these phases at depth releases more K (Tatsumi and Eggins, 1995). Taal is located 200 km above the slab and at Laguna this distance is even greater (Cardwell et al., 1980). Underneath these volcanic centers, melts are generated from small degrees of partial melting in the mantle wedge at high pressure. The basalt melts then rise and stall beneath the crust due to a buoyancy difference. Here it could crystallize and melt the surrounding crust composed of earlier crystallized intrusions. The melts that have now undergone some degree of differentiation, rise again and stall in mid-crust where they can cause partial melting of previously emplaced magma. Previous intrusions that are being partially melted by the new basalt intrusion are also subduction related. The earlier intrusions are varied, being the result of accumulation through time. Excluding the agglomerated terranes, the whole Philippine arc most probably developed from the Philippine Sea Basaltic crust and this crust has since been modified by subduction processes. The crustal rocks that were melted are unlikely to be the original basaltic crust. The new partial melts and the residual basaltic to basaltic andesite melts from the

most recent intrusion mingled/mixed in the reservoir. After some time, another batch of melt from the mantle is intruded into the crustal reservoir. These melts are less alkali compared to the previous basalt intrusion. The different composition of the later basalt intrusion could be due to higher degrees of partial melting and/or a different mantle source. These melts mingled/mixed less with the crustal melts probably because there was less time for mingling prior to being erupted. Ponding of the melts in the lower crust and mid-crust is based on the interpretation that most melts crystallized at a shallower level. The choice of depth is based on a study that identified a low velocity zone beneath southwest Luzon, i.e., at around 18 or 22 km, and the moho at 34 or 32 km depth (Besana et al., 1995). A large percentage of the magma that was erupted as the upper Dilman Tuff probably originated from the mid-crust or shallower levels.

The actual vent where the upper Diliman Tuff was erupted from is unknown. High LILE concentrations (similar with Laguna tuffs) indicate that the source is not along the Bataan arc. The source instead, could be in the same tectonic setting as Laguna or Taal, which means in the region of Macolod Corridor. Magma ascent was, most likely influenced by structures in the area.

Conclusions

The source of the upper pyroclastic flow deposit in Manila is chemically distinct from Laguna and Taal sources. They cannot be related by fractional crystallization, and there are differences in the degrees of partial melting for each source, which may or may not reflect across arc variation. The higher LILE concentrations of the pumice samples in the upper Diliman Tuff relative to Taal can be interpreted to result from lower degrees of partial melting in the source for the upper Diliman Tuff.

The basaltic to dacitic magma that was erupted as pyroclastic flows (upper Diliman Tuff) represent mingled and mixed melts generated by different degrees of partial melting. These melts were produced from melting of both the mantle wedge and a modified crust. Some basaltic intrusions are probably partial melts originating in the mantle wedge fluxed by fluids from dehydration reactions at greater depths. Fluids are mainly introduced from subduction processes. Partial melting in the mantle wedge could occur in different degrees or at different source regions producing the variation in the basaltic melts. These melts rise and stall at the base of the crust where they can melt surrounding crust and further differentiate before rising to shallower levels. The melts can stall again at mid-crust below less dense, and probably more differentiated, materials that could be more easily melted. The less mafic materials in the crust are probably previous intrusions of subduction related magma that have accumulated and stalled through time resulting in some heterogeneity in the crust. Before eruption, as the magma rose, the melts mingled thus producing the varied composition deposit. Pathways for the magma before eruption could be related to the extensional environment in southwest Luzon.

Table 1
Sample Location

Sample	Site	UTM Coordinates	
PIVS1-9.28-A	Diliman, QC		
PIVS1-9.28-B	Diliman, QC		
PIVS1-9.48-A	Diliman, QC		
PIVS1-10.97-A	Diliman, QC		
BH01-01-S1	Novaliches, QC		
BH01-01-P2	Novaliches, QC		
BH07-03-S1	West Triangle, QC		
BH07-03-P1	West Triangle, QC		
BH07-03-P2	West Triangle, QC		
BH07-03-P3	West Triangle, QC		
BH07-03-A	West Triangle, QC		
BH07-03-C	West Triangle, QC		
BH16-(4-5)-A	Valle Verde 4, Pasig		
BH16-(4-5)-B	Valle Verde 4, Pasig		
BH16-(4-5)-C	Valle Verde 4, Pasig		
BH16-(4-5)-D	Valle Verde 4, Pasig		
BH16-(4-5)-E	Valle Verde 4, Pasig		
BH16-(4-5)-F	Valle Verde 4, Pasig		
040303-1A	La Vista gate	293.739	1620.799
040303-1B	La Vista gate		
040303-1C	La Vista gate		
040303-1D	La Vista gate		
040303-1E	La Vista gate		
040303-1F	La Vista gate		
040303-1G	La Vista gate		
040303-1H	La Vista gate		
040303-1I	La Vista gate		
040303-1K	La Vista gate		
040303-1M	La Vista gate		
040303-1N	La Vista gate		
040303-2A	ULTRA-wall	291.815	1612.523
040303-2B	ULTRA-wall		
040303-2C	ULTRA-wall		
040303-2D	ULTRA-wall		
040303-2F	ULTRA-wall		
040303-2G	ULTRA-wall		
040303-3A	Kalayaan road	291.177	1610.35
040303-3B	Kalayaan road		
040303-3C	Kalayaan road		
040303-3E	Kalayaan road		
040303-3F	Kalayaan road		

Table 2
Bulk rock major and trace element concentrations

Sample	PIVS1-9.28-A	PIVS1-9.28-B	PIVS1-9.48-A	PIVS1-10.97-A	BH01-01-S1	BH01-01-P2
SiO_2	52.62	59.49	53.74	54.65	60.74	65.79
TiO_2	1.07	1.03	1.07	1.09	1.01	0.55
Al_2O_3	17.24	16.75	17.11	17.42	17.14	18.42
Fe_2O_3	10.47	7.43	10.28	9.36	6.4	6.2
MnO	0.18	0.2	0.19	0.19	0.22	0.21
MgO	3.49	2.09	3.28	2.98	1.95	3.53
CaO	9.05	4.89	8.28	7.82	4.21	2.62
Na_2O	2.82	4.36	2.95	3.33	4.25	0.81
K_2O	1.94	3.21	2.18	2.31	3.62	1.8
P_2O_5	1.1	0.56	0.93	0.86	0.46	0.06
Totals	98	99	98	98	97	95
Rb (XRF)	55	95	65	69	103	57
Zr (XRF)	105	182	118	126	209	354
Sr (XRF)	672	695	666	688	582	265
V	287.39	62.21	262.53	237.45	44.81	69.72
Cr	0	3.47	0	0	3.37	2.79
Y	29.6	36.74	32.3	31.44	36.03	11.18
Nb	5.35	9.33	5.87	6.61	9.9	10.26
Ba	624.54	983.7	643.3	718.64	1044.53	584.13
La	30.3	39.6	32.32	31.65	39	19.77
Ce	52.04	76.11	57.44	58.65	77.1	48.57
Pr	7.07	9.88	7.85	7.99	9.94	5.27
Nd	30.61	41.62	34.09	34.93	41.37	19.53
Sm	6.73	8.89	7.42	7.43	8.54	4.52
Eu	1.87	2.5	2.07	2.06	2.38	1.06
Gd	6.41	8.17	7.04	6.89	7.99	3.51
Tb	0.9	1.14	0.98	0.98	1.15	0.52
Dy	5.03	6.24	5.54	5.38	6.25	2.33
Ho	1.02	1.27	1.11	1.07	1.24	0.44
Er	2.77	3.54	2.95	2.92	3.42	1.38
Yb	2.85	3.63	3.05	2.88	3.61	1.82
Lu	0.41	0.54	0.44	0.43	0.52	0.24
Hf	3.16	5.24	3.4	3.41	5.54	10.34
Ta	0.34	0.55	0.37	0.37	0.58	1.08
Pb	9.3	18.62	8.95	11.32	22.26	13.68
Th	8.7	14.66	9.47	10.17	15.79	28.17
U	2.61	3.51	2.96	2.68	3.94	1.78

Table 2 continued
Bulk rock major and trace element concentrations

Sample	BH07-03-S1	BH07-03-P1	BH07-03-P2	BH07-03-P3	BH07-03-A	BH07-03-C
SiO_2	59.54	63.25	64.53	61.23	58.8	57.42
TiO_2	0.96	0.88	0.81	0.95	0.98	1.01
Al_2O_3	16.2	16.39	16.63	16.29	16.15	16.47
Fe_2O_3	7.91	5.93	5.36	7.36	8.24	8.95
MnO	0.2	0.26	0.2	0.21	0.27	0.2
MgO	2.49	1.94	1.55	2.31	2.62	2.98
CaO	5.48	3.79	2.96	4.69	5.72	6.47
Na_2O	3.83	3.83	3.79	3.54	3.77	3.44
K_2O	2.92	3.42	3.92	3	2.92	2.47
P_2O_5	0.47	0.32	0.26	0.42	0.53	0.58
Totals	98	97	96	97	98	99
Rb (XRF)	82	89	98	77	78	68
Zr (XRF)	156	206	220	174	153	132
Sr (XRF)	535	417	382	465	523	586
V	172.35	77.87	82.34	114.28	173.17	200.23
Cr	3.05	3.38	3.48	3.16	3.15	3.3
Y	35.4	33.71	34.21	33.6	34.92	34.75
Nb	8.52	10.55	12.21	8.88	7.94	7.06
Ba	873.81	1042.46	1121.07	894.5	841.17	768.16
La	31.77	32.55	37.11	32.57	31.61	29.24
Ce	62.13	70.56	79.24	64.67	60.86	57.61
Pr	8.18	8.15	9.31	8.21	8.02	7.7
Nd	35.03	32.99	36.99	34.47	34.55	33.05
Sm	8.65	7	8.67	7.6	8.65	7.74
Eu	2.23	1.81	2.23	2.02	2.21	2.09
Gd	7.57	6.35	7.44	7.01	7.42	7.35
Tb	1.13	0.94	1.14	1.02	1.12	1.05
Dy	6.28	5.36	6	5.66	5.9	5.85
Ho	1.26	1.05	1.19	1.16	1.22	1.13
Er	3.9	3	3.93	3.18	3.87	3.3
Yb	4.57	3.36	4.91	3.31	4.48	3.58
Lu	0.67	0.48	0.7	0.49	0.65	0.51
Hf	5.47	5.61	6.64	5.09	5.13	4.12
Ta	0.6	0.53	0.86	0.54	0.56	0.36
Pb	14.6	21.99	26.48	17.16	13.87	12.12
Th	12.2	14.34	15.95	12.75	11.43	10.7
U	2.69	3.02	3.75	2.7	2.71	2.22

Table 2 continued
Bulk rock major and trace element concentrations

Sample	BH16-(4-5)-A	BH16-(4-5)-B	BH16-(4-5)-C	BH16-(4-5)-D	BH16-(4-5)-E	BH16-(4-5)-F
SiO_2	64.48	61.34	61.92	61.39	63.35	61.1
TiO_2	0.84	1.01	0.92	0.92	0.86	0.93
Al_2O_3	16.62	16.71	17.2	16.86	16.31	16.64
Fe_2O_3	5.75	8.81	7.75	7.63	5.97	7.97
MnO	0.21	0.12	0.13	0.18	0.2	0.17
MgO	1.25	1.48	1.35	1.89	1.56	2
CaO	3.06	4.82	4.2	4.68	3.68	4.9
Na_2O	3.73	2.88	3.45	3.28	4.16	3.15
K_2O	3.77	2.42	2.73	2.79	3.57	2.73
P_2O_5	0.3	0.4	0.35	0.39	0.35	0.41
Totals	96	97	98	98	97	98
Rb (XRF)	105	66	77	74	96	96
Zr (XRF)	212	137	169	174	194	194
Sr (XRF)	408	632	587	565	439	439
V	70.75	111.54	107.62	142.05	124.62	83.73
Cr	0	0	8.8	9.74	10.06	0
Y	33.91	22.16	28.47	30.04	22.42	33.76
Nb	12.6	6.75	8.97	9.79	7.96	11.38
Ba	1138.8	779.77	945.11	929.65	710.78	1023.87
La	37.58	24.99	30.18	30.71	23.31	36.71
Ce	79.03	44.69	58.34	64.23	49.18	72.18
Pr	9.32	5.9	7.45	8.05	6.08	9.04
Nd	37.01	24.48	29.7	33.45	24.81	36.31
Sm	7.89	5.36	6.53	9.19	7.41	7.8
Eu	2.22	1.47	1.88	2.54	2	2.14
Gd	7.06	4.82	6.3	7.86	6.25	7.02
Tb	1.06	0.71	0.89	1.25	1	1.06
Dy	5.74	3.83	4.94	6.44	5.2	5.6
Ho	1.19	0.77	0.96	1.3	1.1	1.18
Er	3.44	2.17	2.81	4.64	3.89	3.3
Yb	3.79	2.29	2.86	5.23	4.41	3.52
Lu	0.54	0.34	0.44	0.81	0.69	0.54
Hf	5.04	4.24	4.03	5.53	4.71	4.98
Ta	0.68	0.5	0.53	0.94	0.83	0.62
Pb	26.24	12.1	21.89	24.36	18.82	22.77
Th	14.4	11.27	12.34	12.42	9.59	13.56
U	4.52	2.17	3.42	3.53	3.27	3.96

Table 2 continued
Bulk rock major and trace element concentrations

Sample	040303-1A	040303-1B	040303-1C	040303-1D	040303-1E	040303-1F
SiO_2	51.84	50.94	60.91	58.89	51.27	52.89
TiO_2	1.18	1.16	1.02	1.04	1.17	1.21
Al_2O_3	18.24	18.75	17.04	17.04	18.3	19.34
Fe_2O_3	12.24	10.64	6.68	7.57	11.08	11.48
MnO	0.18	0.33	0.25	0.35	0.15	0.12
MgO	3.01	2.33	1.69	2.14	2.57	1.36
CaO	8.63	9.42	4.22	5.03	9.62	8.14
Na_2O	2.51	2.78	4.22	4.11	2.71	2.81
K_2O	0.93	1.08	3.47	3.2	1.09	1.17
P_2O_5	1.25	2.57	0.5	0.64	2.03	1.48
Totals	96	96	98	98	96	96
Rb (XRF)	41	41	106	92	32	40
Zr (XRF)	119	144	199	184	130	125
Sr (XRF)	712	802	604	635	761	789
V	273.38	226.84	50.18	87.98	259.42	332.63
Cr	4.23	3.63	3.04	2.74	3.82	4.42
Y	46.58	45.89	35.26	35.36	39.73	72
Nb	5.54	6.44	10.24	9.33	5.87	6.08
Ba	649	907.6	1095.96	1110.49	744.9	744.35
La	39.33	43.85	39.76	36.71	37.42	55.14
Ce	64.08	71.64	78.58	73.38	57.88	58.02
Pr	9.13	9.98	9.78	9.28	8.49	10.39
Nd	40.15	43.79	39.7	38.62	37.31	45.42
Sm	9.74	10.67	9.47	9.44	9.03	9.76
Eu	2.58	2.77	2.4	2.39	2.35	2.56
Gd	9.18	9.55	7.86	8.05	8.16	10.16
Tb	1.29	1.34	1.17	1.19	1.16	1.33
Dy	7.08	7.28	6.11	6.2	6.22	7.56
Ho	1.43	1.46	1.21	1.27	1.24	1.62
Er	4.4	4.47	3.73	3.84	3.89	4.84
Yb	5.02	5.08	4.53	4.55	4.47	4.78
Lu	0.75	0.75	0.68	0.66	0.64	0.69
Hf	3.9	4.56	6.12	5.65	4.02	3.68
Ta	0.4	0.48	0.68	0.59	0.4	0.3
Pb	9.39	9.5	26.1	16.24	8.69	9.12
Th	8.84	10.37	15.4	13.67	9.04	9.54
U	2.97	7.54	3.48	3.14	6.41	3.55

Table 2 continued
Bulk rock major and trace element concentrations

Sample	040303-1G	040303-1H	040303-1I	040303-1K	040303-1M	040303-1N
SiO_2	51.66	50.41	51.84	50.4	50.18	56.1
TiO_2	1.16	1.31	1.19	1.22	1.08	1.11
Al_2O_3	18.39	20.12	19.17	18.88	17.48	18.53
Fe_2O_3	11.03	12.14	10.94	11.45	10.8	9.16
MnO	0.15	0.23	0.21	0.21	0.16	0.29
MgO	2.7	2.71	1	2.38	3.05	2.32
CaO	9.42	8.3	8.73	9.6	10.98	5.59
Na_2O	2.62	2.64	2.92	2.61	2.55	3.7
K_2O	1.11	1.02	1.35	1.1	0.93	2.33
P_2O_5	1.75	1.14	2.66	2.13	2.78	0.87
Totals	97	95	96	96	98	97
Rb (XRF)	36	38	40	45	25	78
Zr (XRF)	124	132	136	125	121	168
Sr (XRF)	738	699	800	761	756	662
V	277.75	275.95	290.06	263.16	311.75	105.74
Cr	5.52	4.69	3.35	3.86	5.78	2.77
Y	40.41	38.74	38.14	38.2	34.07	40.77
Nb	5.89	6.42	6.29	5.83	5.23	8.61
Ba	666.74	692.01	898.03	762.46	633.6	883.93
La	35.73	36.4	37.05	35.84	32.98	37.44
Ce	57.19	62.87	61.8	59.12	56.07	72.5
Pr	8.47	8.99	8.7	8.36	7.62	9.85
Nd	37.18	39.36	37.69	37.14	33.1	43.27
Sm	9.18	9.72	9.43	9.17	8.03	10.63
Eu	2.4	2.53	2.44	2.35	2.15	2.78
Gd	8.18	8.57	8.18	8.03	7.45	9.22
Tb	1.18	1.23	1.18	1.14	1.04	1.32
Dy	6.43	6.73	6.39	6.32	5.59	7.3
Ho	1.27	1.31	1.27	1.27	1.1	1.45
Er	4.03	3.97	3.84	3.79	3.47	4.47
Yb	4.56	4.6	4.42	4.33	3.94	4.98
Lu	0.67	0.66	0.64	0.63	0.58	0.73
Hf	3.96	4.42	4.7	4.2	3.82	5.64
Ta	0.39	0.45	0.48	0.42	0.4	0.6
Pb	8.7	12.88	9.74	9.4	8.06	15.88
Th	8.9	10.17	10.83	9.37	8.64	14.19
U	5.78	4.73	4.6	5.56	6.19	3.19

Table 2 continued
Bulk rock major and trace element concentrations

Sample	040303-2A	040303-2B	040303-2C	040303-2D	040303-2F	040303-2G
SiO_2	60.66	63.07	62.9	62.15	64.12	63.09
TiO_2	0.92	0.84	0.87	0.86	0.84	0.85
Al_2O_3	16.11	16.13	16.3	16.19	16.59	16.22
Fe_2O_3	7.31	5.84	6.04	6.31	5.67	5.87
MnO	0.2	0.2	0.2	0.19	0.17	0.19
MgO	2.17	1.55	1.71	1.71	1.43	1.6
CaO	4.93	3.95	3.94	4.22	3.02	3.68
Na_2O	4.11	4.23	4.14	4.39	3.62	4.53
K_2O	3.16	3.58	3.52	3.46	4.21	3.61
P_2O_5	0.44	0.6	0.37	0.52	0.32	0.36
Totals	99	97	96	98	97	98
Rb (XRF)	83	97	95	87	99	95
Zr (XRF)	167	201	193	184	210	194
Sr (XRF)	489	431	423	483	394	430
V	137.2	80.82	82.07	96.27	70.38	86.71
Cr	3.36	3.82	2.87	2.68	3.23	3.96
Y	35.12	38.2	35.99	36.71	36.94	35.48
Nb	8.83	11.06	10	9.87	11.03	11.22
Ba	906.06	1079.72	1006.97	1005.31	1101.37	1054.15
La	33.01	39.11	35	35.57	37.94	35.72
Ce	65.45	75.6	68.91	69.68	76.45	74.12
Pr	8.34	9.61	8.71	8.89	9.43	9.21
Nd	34.64	39.48	35.95	37.28	37.79	37.34
Sm	8.74	9.49	8.71	9.09	8.1	8.98
Eu	2.21	2.4	2.22	2.35	1.93	2.28
Gd	7.54	8.17	7.66	7.84	7.33	7.53
Tb	1.11	1.24	1.16	1.19	1.03	1.14
Dy	6.22	6.48	6.24	6.31	5.73	6.28
Ho	1.26	1.32	1.28	1.29	1.14	1.26
Er	3.99	4.26	3.98	4.16	3.41	4.06
Yb	4.81	5.07	4.74	4.92	3.95	4.9
Lu	0.71	0.77	0.71	0.72	0.54	0.71
Hf	5.52	6.55	6.06	6	5.8	5.7
Ta	0.62	0.76	0.71	0.69	0.58	0.73
Pb	36.85	29.5	24.6	19.86	27.09	39.39
Th	12.6	15.28	14.2	13.83	16.06	13.52
U	2.91	4.26	3.21	3.31	3.59	3.77

Table 2 continued
Bulk rock major and trace element concentrations

Sample	040303-3A	040303-3B	040303-3C	040303-3E	040303-3F
SiO_2	63.29	63.33	61.99	58.71	61.67
TiO_2	0.83	0.85	0.89	0.92	0.9
Al_2O_3	16.33	16.01	16.27	16.47	16.33
Fe_2O_3	5.74	5.88	6.56	7.85	6.69
MnO	0.19	0.2	0.2	0.24	0.19
MgO	1.51	1.53	1.74	2.48	1.84
CaO	3.62	3.82	4.34	6.06	4.45
Na_2O	4.34	4.24	3.97	3.69	4.01
K_2O	3.76	3.71	3.48	2.92	3.42
P_2O_5	0.38	0.44	0.57	0.66	0.51
Totals	97	97	97	98	97
Rb (XRF)	105	110	102	85	102
Zr (XRF)	217	217	202	174	197
Sr (XRF)	420	436	463	536	494
V	58.58	63.89	102.65	132.19	89.4
Cr	3.4	4.61	5.03	4.24	4
Y	36.44	37.78	37.04	36.63	37.85
Nb	11.35	11.72	10.03	8.84	10.26
Ba	937.33	1010.33	918.5	818.31	856.2
La	33.43	35.08	32.37	30.67	32.6
Ce	69.38	72.42	65.09	60.79	64.39
Pr	8.52	9.12	8.22	8.13	8.22
Nd	34.36	37.38	34.13	34.96	34.79
Sm	7.42	9.13	7.81	8.77	8.08
Eu	1.91	2.3	1.99	2.22	2.04
Gd	6.8	7.92	7.12	7.64	7.11
Tb	0.99	1.2	1.07	1.17	1.06
Dy	5.6	6.65	5.96	6.37	6.02
Ho	1.12	1.34	1.18	1.28	1.2
Er	3.29	4.32	3.54	4.07	3.61
Yb	3.82	5.1	4.02	4.75	4.06
Lu	0.53	0.75	0.58	0.71	0.58
Hf	5.44	6.84	5.36	5.87	5.72
Ta	0.54	0.77	0.52	0.63	0.54
Pb	23.69	27.7	31.42	17.88	18.12
Th	13.02	14.06	12.6	11.48	12.51
U	3.57	4.02	3.29	3.07	3.09

Table 3
Plagioclase compositions

Sample	SiO_2	Al_2O_3	FeO	CaO	Na_2O	K_2O	Total	%An
PIVS1-9.28A-pl9	46.07	32.72	0.77	17.23	1.52	0.06	98.49	85.46
PIVS1-9.28A-pl10-c	45.75	33.78	0.68	17.99	1.33	0.11	99.69	89.25
PIVS1-9.28A-pl10-r	45.38	33.72	0.77	18.16	1.24	0.07	99.96	90.07
PIVS1-9.28A-pl11-c	51.30	29.93	0.73	13.67	3.78	0.26	99.87	67.80
PIVS1-9.28A-pl11-r1	48.25	31.87	0.80	16.13	2.29	0.11	99.56	80.03
PIVS1-9.28A-pl11-r2	47.42	31.41	0.81	15.83	2.28	0.14	98.03	78.51
Enclave (e1-e3)								
PIVS1-9.28A-e1-pl1-c	53.38	28.41	0.57	11.76	4.72	0.34	99.49	58.34
PIVS1-9.28A-e1-pl1-r1	50.73	29.99	0.51	13.81	3.61	0.26	99.07	68.50
PIVS1-9.28A-e1-pl1-r2	53.16	28.48	0.61	11.77	4.56	0.47	99.20	58.41
PIVS1-9.28A-e1-pl2	50.63	30.69	0.52	13.69	3.56	0.22	99.56	67.93
PIVS1-9.28A-e1-pl3	53.82	28.02	0.63	11.02	5.08	0.38	99.11	54.69
PIVS1-9.28A-e1-pl4	54.31	26.73	0.54	10.59	5.32	0.42	98.89	52.55
PIVS1-9.28A-e2-pl7	55.28	26.67	0.56	10.02	5.49	0.71	98.83	49.73
PIVS1-9.28A-e3-pl5-c	44.13	34.50	0.59	18.85	0.81	0.04	99.01	93.52
PIVS1-9.28A-e3-pl5-r1	45.73	33.59	0.85	17.65	1.35	0.04	99.28	87.57
PIVS1-9.28A-e3-pl5-r2	44.32	35.07	0.61	18.86	0.67	0.05	99.70	93.55
PIVS1-9.28A-e3-pl6-c	44.61	32.90	1.02	17.44	0.97	0.11	97.34	86.52
PIVS1-9.28A-e3-pl6-r1	48.48	31.30	1.29	15.36	2.57	0.11	99.26	76.21
PIVS1-9.28A-e3-pl6-r2	45.07	34.01	0.83	18.69	1.12	-0.01	99.98	92.73
BH0703-P3-pl1-c	52.44	28.25	0.56	11.35	4.81	0.29	97.84	56.31
BH0703-P3-pl1-r	55.22	26.90	0.56	10.30	5.28	0.35	98.77	51.10
BH0703-P3-pl2-c	53.81	28.07	0.59	11.11	5.01	0.35	99.17	55.12
BH0703-P3-pl2-r	54.89	27.28	0.50	10.56	5.32	0.34	99.83	52.39
040303-1N-pl1-c	49.35	30.99	0.57	14.86	2.83	0.12	98.90	73.72
040303-1N-pl1-r1	47.53	32.08	0.57	15.96	2.36	0.13	98.91	79.18
040303-1N-pl1-i	47.96	32.41	0.61	16.50	2.07	0.10	100.03	81.88
040303-1N-pl3	47.41	32.22	0.75	16.07	2.21	0.17	98.92	79.73
040303-2C-pl3	59.82	25.34	0.42	7.21	7.10	0.77	101.52	35.74
040303-2C-pl4	55.61	28.21	0.50	10.89	5.45	0.33	101.38	54.05
040303-2F-pl1	58.69	25.89	0.54	8.54	6.02	0.58	100.53	42.39
040303-3B-pl1-c	51.71	29.05	0.65	12.46	4.25	0.29	98.65	61.84
040303-3B-pl1-r1	53.99	27.91	0.52	10.96	4.83	0.29	98.67	54.38
040303-3B-pl1-r2	54.97	26.87	0.59	10.24	5.41	0.40	98.60	50.81
040303-3B-pl2-c	54.30	28.05	0.55	10.72	5.17	0.38	99.39	53.18
040303-3B-pl2-r1	54.51	27.77	0.51	10.59	5.44	0.44	99.63	52.54
040303-3B-pl3-c	55.93	27.10	0.53	10.35	5.60	0.43	100.04	51.36
040303-3B-pl3-r1	54.97	27.66	0.57	10.70	5.18	0.40	99.90	53.07

Table 3 continued
Plagioclase compositions

Sample	SiO_2	Al_2O_3	FeO	CaO	Na_2O	K_2O	Total	%An
040303-3F-pl1-c	53.38	28.53	0.54	11.51	4.64	0.30	99.00	57.10
040303-3F-pl1-r1	52.87	28.92	0.51	12.23	4.56	0.32	100.30	60.68
040303-3F-pl1-r2	53.55	28.21	0.56	11.45	4.37	0.30	98.86	56.80
040303-3F-pl2	53.70	28.66	0.59	11.88	4.80	0.35	100.21	58.96
040303-3F-pl3-c	52.47	27.91	0.61	11.25	4.80	0.35	97.53	55.84
040303-3F-pl3-r1	52.05	28.23	0.63	12.31	4.35	0.31	98.30	61.09
040303-3F-pl3-r2	54.10	27.98	0.50	10.94	5.22	0.39	99.32	54.28

Table 3 continued
Pyroxene compositions

Sample	SiO_2	Al_2O_3	TiO_2	FeO	MnO	MgO	CaO	Na_2O	Total	Wo%	En%	Fs%	Al/Ti	Mg#
PIVS1-9.28A-px6	50.69	4.11	0.60	8.58	0.18	14.52	21.91	0.29	100.92	44.90	41.38	13.72	6.08	62.85
PIVS1-9.28A-px7	51.46	2.81	0.62	10.57	0.29	14.99	19.80	0.37	100.95	40.49	42.64	16.87	4.03	58.64
PIVS1-9.28A-px8	51.45	3.11	0.71	8.93	0.37	14.57	21.21	0.35	100.73	43.78	41.84	14.39	3.89	62.00
PIVS1-9.28A-e1-px2	51.84	2.02	0.27	11.65	0.56	14.91	18.98	0.30	100.52	38.88	42.49	18.63	6.66	56.14
PIVS1-9.28A-e1-px3	51.75	2.06	0.33	12.03	0.50	14.44	19.18	0.31	100.65	39.42	41.29	19.30	5.48	54.55
PIVS1-9.28A-e1-px1	51.98	2.18	0.31	11.03	0.45	14.77	19.27	0.33	100.36	39.79	42.43	17.79	6.14	57.23
PIVS1-9.28A-e3-px4	50.78	2.71	0.70	11.99	0.37	14.76	18.90	0.38	100.63	38.73	42.09	19.18	3.42	55.18
PIVS1-9.28A-e3-px5	52.05	1.55	0.46	12.33	0.43	15.81	17.54	0.31	100.49	35.68	44.74	19.58	2.98	56.18
BH07-03-P3-px1	52.04	1.57	0.49	9.04	0.68	15.66	18.80	0.35	98.64	38.46	45.73	14.81	2.86	63.40
BH07-03-P3-px2	53.72	1.36	0.32	16.54	1.00	25.05	2.28	0.05	100.33	4.55	69.65	25.80	3.71	60.24
BH07-03-P3-px3	51.38	2.52	0.61	8.61	0.58	15.26	20.19	0.41	99.58	41.94	44.10	13.95	3.64	63.94
BH07-03-P3-px5	53.54	1.02	0.29	17.21	1.33	24.30	1.70	0.04	99.56	3.48	69.07	27.45	3.10	58.54
040303-1N-px2	50.49	1.87	0.48	10.49	0.60	14.19	18.85	0.37	97.36	40.30	42.20	17.50	3.44	57.49
040303-2C-px1	54.18	0.68	0.17	17.93	1.27	25.09	1.61	0.04	100.97	3.19	69.10	27.71	3.49	58.32
040303-2C-px2	50.47	2.96	0.69	9.06	0.50	14.70	19.87	0.41	98.67	41.93	43.15	14.92	3.81	61.87
040303-2C-px3	49.77	3.17	0.91	9.56	0.47	14.75	20.03	0.43	99.09	41.72	42.74	15.54	3.09	60.68
040303-2F-px1	51.06	1.22	0.39	9.82	0.97	14.83	18.39	0.38	97.07	39.40	44.18	16.42	2.76	60.15
040303-3B-px1	52.05	1.90	0.42	8.76	0.42	15.51	20.64	0.30	100.04	42.08	43.98	13.94	4.00	63.90
040303-3B-px2	53.45	0.99	0.29	19.48	1.31	23.91	1.57	0.02	101.03	3.13	66.48	30.39	3.02	55.10
040303-3B-px4	51.89	2.01	0.52	9.65	0.68	15.48	19.64	0.35	100.24	40.32	44.22	15.46	3.42	61.61
040303-3B-px5	51.78	1.69	0.43	9.49	0.55	15.70	19.79	0.33	99.81	40.36	44.53	15.11	3.50	62.31
040303-3F-px1	51.03	2.68	0.64	9.99	0.53	15.49	19.29	0.35	100.05	39.66	44.31	16.03	3.68	60.80
040303-3F-px2	50.71	2.65	0.63	10.06	0.59	15.51	19.05	0.35	99.56	39.29	44.50	16.20	3.70	60.64
040303-3F-px3	53.38	0.62	0.25	20.19	1.52	22.99	1.56	0.05	100.59	3.16	64.88	31.96	2.19	53.25

Table 3 continued
Groundmass Glass compositions

Sample	SiO_2	Al_2O_3	TiO_2	FeO	MnO	MgO	CaO	Na_2O	K_2O	Cl	Cr_2O_3	F	Total
PIVS1-9.28A-gm1	65.05	15.51	0.33	3.00	0.11	0.54	1.33	2.85	7.29	0.08	0.00	0.00	96.10
PIVS1-9.28A-gm2	64.55	15.71	0.29	3.16	0.19	0.77	1.94	2.84	6.54	0.08	0.00	0.00	96.07
PIVS1-9.28A-gm3	66.04	16.25	0.32	3.43	0.09	0.62	1.74	2.57	7.19	0.08	0.00	0.07	98.39
Enclave (e1-e3)													
PIVS1-9.28A-e1-gm1	56.62	14.12	0.75	9.82	0.23	2.59	5.08	2.75	3.92	0.35	0.04	0.06	96.35
PIVS1-9.28A-e1-gm2	56.82	14.38	0.61	9.72	0.16	2.52	4.99	3.09	3.84	0.44	0.00	0.31	96.89
PIVS1-9.28A-e1-gm3	63.74	16.09	0.52	3.35	0.15	0.59	1.75	4.05	6.08	0.13	0.05	0.00	96.51
PIVS1-9.28A-e2-gm1	59.38	21.92	0.15	1.43	0.03	0.12	5.20	5.87	3.37	0.04	0.01	0.11	97.62
PIVS1-9.28A-e2-gm2	60.21	21.88	0.20	1.02	0.01	0.08	4.98	6.01	3.38	0.03	0.02	0.00	97.80
PIVS1-9.28A-e3-gm1	59.30	15.93	0.67	6.08	0.12	0.55	3.47	4.36	3.28	0.13	0.00	0.00	93.89
PIVS1-9.28A-e3-gm2	54.98	27.17	0.02	1.06	0.01	0.15	10.49	5.46	0.56	0.00	0.02	0.00	99.91
BH07-03-P3-gm2	65.99	15.71	0.54	3.08	0.19	0.79	1.82	4.83	3.91	0.19	0.01	0.09	97.15
BH07-03-P3-gm3	59.80	16.14	0.71	5.00	0.19	1.95	4.59	4.39	3.02	0.13	0.05	0.03	95.98
BH07-03-P3-gm4	63.87	16.05	0.60	3.45	0.21	1.14	2.60	4.65	3.95	0.19	0.01	0.05	96.77
BH07-03-P3-gm5	63.24	15.80	0.67	3.86	0.24	1.22	2.75	4.88	3.76	0.17	0.03	0.08	96.69
BH07-03-C-gm1	65.28	15.48	0.57	2.74	0.11	0.56	1.66	4.54	4.25	0.13	0.03	0.12	95.45
BH07-03-C-gm2	64.38	15.59	0.52	2.96	0.15	0.76	2.02	4.52	4.12	0.21	0.00	0.10	95.32
BH07-03-C-gm3	56.72	15.79	0.89	6.25	0.26	2.65	5.47	3.14	2.83	0.13	0.04	0.43	94.60
BH07-03-C-gm4	54.32	16.90	0.95	8.49	0.15	3.83	7.72	4.04	1.70	0.09	0.00	0.00	98.19
BH07-03-C-gm5	62.06	15.78	0.64	4.56	0.22	1.30	3.24	4.31	3.46	0.13	0.00	0.09	95.78
040303-1C-gm1	60.63	17.05	0.71	5.03	0.20	1.63	4.19	4.74	3.76	0.09	0.00	0.05	98.08
040303-1C-gm2	61.74	17.03	0.75	5.21	0.17	1.62	3.76	4.57	3.75	0.10	0.00	0.14	98.84
040303-1C-gm3	62.85	16.47	0.70	4.26	0.14	1.17	3.07	4.50	3.89	0.10	0.05	0.05	97.24
040303-1C-gm4	63.58	16.19	0.63	3.73	0.17	0.73	2.23	4.55	3.93	0.12	0.00	0.04	95.89
040303-1C-gm5	57.51	16.15	0.87	5.94	0.20	2.03	4.29	4.11	3.46	0.10	0.00	0.00	94.66

Table 3 continued
Groundmass Glass compositions

Sample	SiO_2	Al_2O_3	TiO_2	FeO	MnO	MgO	CaO	Na_2O	K_2O	Cl	Cr_2O_3	F	Total
040303-1N-gm1	55.04	16.88	0.91	7.93	0.32	3.17	6.60	3.91	2.90	0.09	0.00	0.09	97.83
040303-1N-gm2	57.52	17.16	0.85	6.22	0.17	2.33	5.79	4.38	3.06	0.07	0.00	0.04	97.58
040303-1N-gm3	55.91	16.89	0.91	7.32	0.23	2.66	6.53	3.88	2.67	0.10	0.01	0.00	97.13
040303-1N-gm4	55.89	17.28	0.95	7.21	0.19	2.89	6.53	4.00	2.54	0.06	0.00	0.00	97.54
040303-2C-gm1	62.81	15.63	0.63	3.91	0.09	1.06	2.91	4.50	3.95	0.18	0.00	0.08	95.75
040303-2C-gm2	61.09	15.95	0.69	4.83	0.16	1.49	3.67	4.50	3.23	0.14	0.06	0.03	95.82
040303-2C-gm4	62.48	15.71	0.64	4.33	0.12	1.32	3.17	4.38	3.50	0.15	0.00	0.00	95.79
040303-2C-gm5	64.06	16.02	0.57	3.50	0.20	1.08	2.36	4.25	3.91	0.21	0.01	0.11	96.30
040303-2C-gm3	61.00	16.08	0.71	5.26	0.22	1.67	3.96	4.52	3.31	0.14	0.03	0.18	97.09
040303-2F-gm1	63.98	16.13	0.61	4.10	0.19	1.21	2.71	3.98	3.79	0.15	0.00	0.00	96.86
040303-2F-gm2	64.93	16.68	0.63	3.87	0.10	1.15	2.71	4.60	3.63	0.18	0.00	0.00	98.49
040303-2F-gm5	63.32	15.22	0.58	3.48	0.15	0.69	2.14	3.31	4.71	0.18	0.01	0.00	93.80
040303-3B-gm1	62.55	15.52	0.56	3.85	0.10	1.03	2.58	3.98	3.97	0.14	0.03	0.00	94.31
040303-3B-gm2	63.29	15.40	0.63	3.68	0.14	0.88	2.39	3.81	3.98	0.14	0.00	0.00	94.33
040303-3B-gm3	62.64	15.48	0.62	3.95	0.17	1.03	2.61	3.92	3.87	0.19	0.00	0.09	94.56
040303-3F-gm1	60.20	15.82	0.66	4.64	0.20	1.41	3.52	3.92	3.72	0.15	0.00	0.01	94.25
040303-3F-gm2	59.39	15.73	0.65	4.38	0.15	1.58	4.14	4.11	3.34	0.13	0.02	0.11	93.72
040303-3F-gm3	59.70	16.12	0.63	4.96	0.13	1.64	4.21	3.95	3.25	0.13	0.03	0.18	94.93
040303-3F-gm4	60.04	15.76	0.61	5.11	0.16	1.61	3.96	4.23	3.31	0.17	0.00	0.00	94.96
040303-3F-gm5	59.18	15.95	0.70	5.28	0.16	1.91	4.48	4.17	3.05	0.14	0.03	0.00	95.06

Table 3 continued
Oxide compositions

Sample	SiO_2	Al_2O_3	TiO_2	FeO	MnO	MgO	CaO	V_2O_3	Cr_2O_3	Total
PIVS1-9.28A-e1-mt1	0.16	4.27	7.32	78.21	0.42	2.97	0.22	0.24	0.01	93.81
PIVS1-9.28A-e1-mt2	0.19	4.39	7.54	79.56	0.45	3.11	0.12	0.30	0.05	95.70
PIVS1-9.28A-mt3	0.11	5.36	7.10	78.40	0.33	4.23	0.06	0.73	0.08	96.40
040303-3B-mt1	0.17	3.44	11.97	72.49	0.86	3.82	0.15	0.25	0.08	93.23
040303-3B-mt2	0.10	2.69	11.87	75.83	0.84	2.89	0.09	0.22	0.03	94.56
040303-2C-mt1	0.07	3.14	10.88	76.63	0.87	3.50	0.05	0.27	0.00	95.42
040303-2C-mt2	0.08	3.27	10.69	77.23	0.85	3.49	0.01	0.22	0.04	95.87

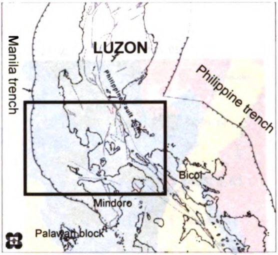

Figure 1a. Tectonic setting of the northern half of the Philippines, showing the location of opposing subduction zones (Manila Trench and Philippine Trench) and the left lateral Philippine Fault in between. The enclosed area is enlarged in the next map (Fig. 1b) and includes southwest Luzon and the study area.

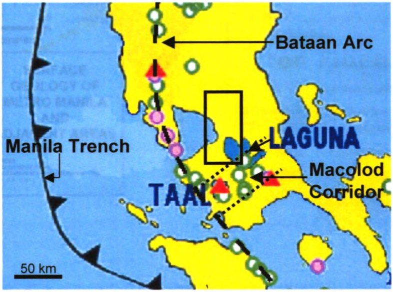

Figure 1b. A map showing the west facing volcanic arc, Bataan Arc (dashed line), and the location of Macolod corridor. The symbols represent active (triangle), potentially active (filled circle), and inactive (open circle) volcanoes. Taal and Laguna calderas are labeled. The enclosed area covers the extent of the surface geologic map of Metro Manila shown in figure 2.

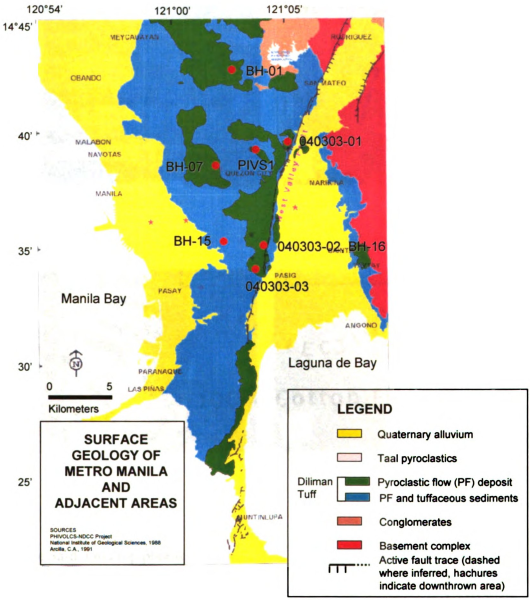

Figure 2. Surface geology map of Metro Manila. The upper Diliman Tuff is shown in green. Sample location is indicated by red circles and beside it is the site number.

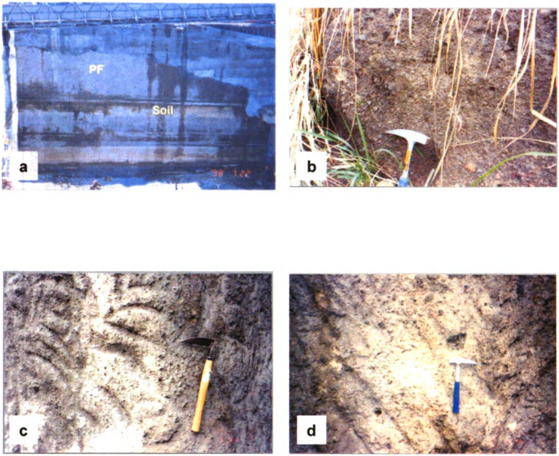

Figure 3a-d. Outcrop photos

a. An excavation for a building showing an approximately 10 m thick pyroclastic flow (PF) deposit and other units below. This is located in Cubao, Quezon City. The upper pyroclastic flow deposit is correlated with the upper Diliman Tuff and although this site was not sampled, it shows a thickness for the unit and other deposits below

b. Pyroclastic flow deposit sampled in site 040303-01 (Brgy. Malanday, Quezon City).

c. Pyroclastic flow deposit sampled in site 040303-02 (ULTRA, Pasig).

d. Pyroclastic flow deposit sampled in site 040404-03 (Kalayaan Ave., Pasig).

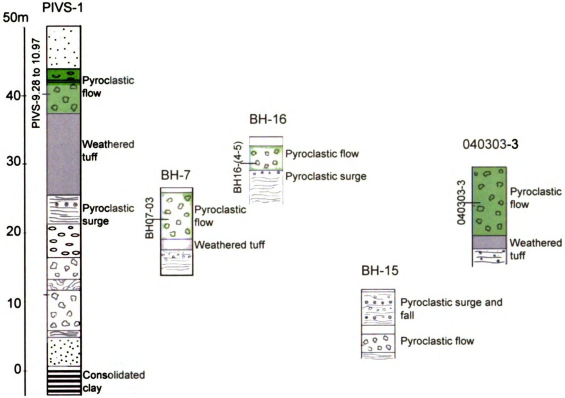

Figure 4. Stratigraphic logs of selected sample sites. Correlation of the upper Diliman Tuff unit (shaded green) is shown.

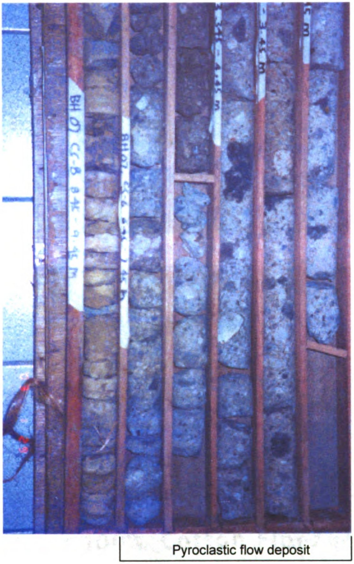

Figure 5. Photo of a core sample (BH-07). The unit contains heterogenous pumice clasts - mafic, felsic and banded pumice.

Figure 6. A close-up of the core samples from PIVS1-9.28 (a) and BH-07 (b). Two clasts, a mafic (dark) and felsic (light) pumice clast, in BH-07 are outlined.

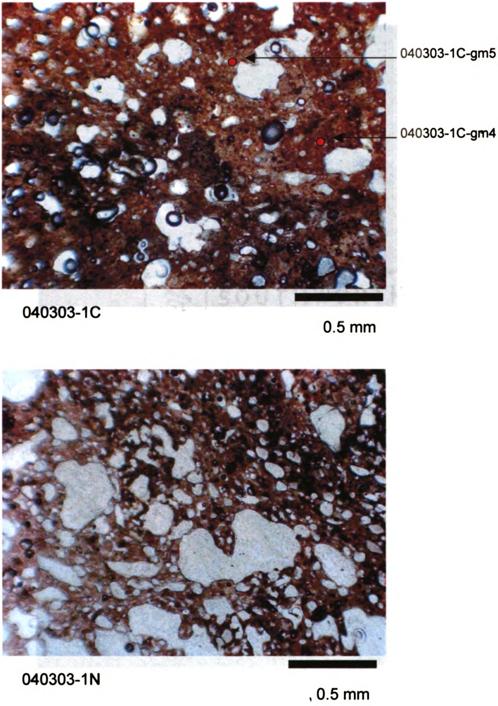

Figure 7. Photograph of groundmass in plane polarized light showing vesiculation and mingling (dark and light glass). For pumice 040303-1C the points with analysis are shown (see table 3).

040303-3B

0.5 mm

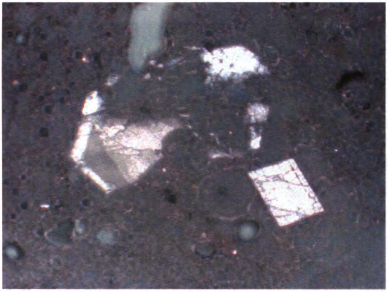

BH07-03-P3

1 mm

Figure 8. Photos in crossed polars of plagioclase as glomerocryst and isolated phenocrysts. Zoning can be seen. The groundmass is mostly glass with crystallites.

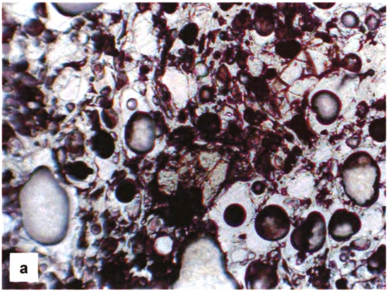

040303-2C

0.1 mm

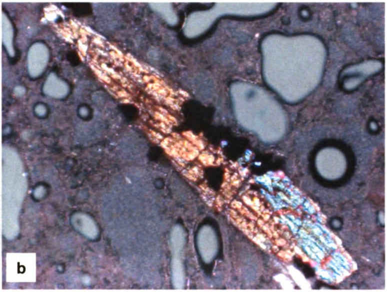

040303-2C

0.5 mm

Figure 9. Pyroxenes in sample 040303-2C, a clinopyroxene in plane polarized light (a) and an othopyroxene in crossed polars (b) with magnetite inclusions.

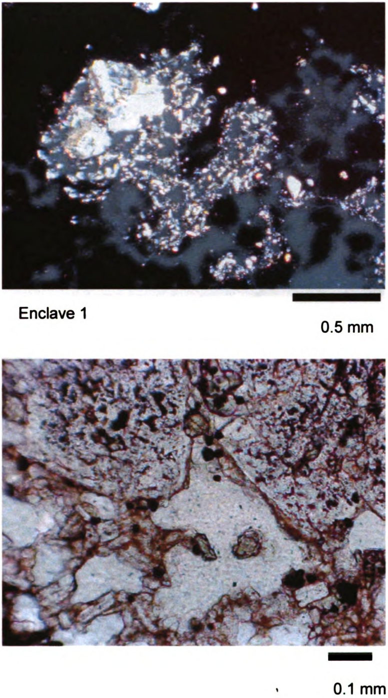

Figure 10. A photo of enclave 1 in PIVS1-9.28A showing microlitic groundmass of mostly plagioclase and plagioclase glomerocryst in crossed polars. The close up of plagioclase phenocrysts in this enclave, shows numerous inclusions and rounded grain edges.

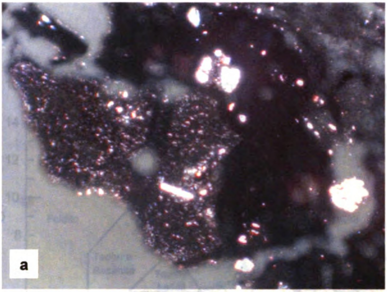

Enclave 2

1 mm

Enclave 3

0.5 mm

Figure 11.
a. Enclave 2 in PIVS1-9.28A under crossed polars showing acicular crystallites in the groundmass and one larger plagioclase lath.
b. Enclave 3 in PIVS1-9.28A under plane polarized light containing zoned plagioclase and clinopyroxene.

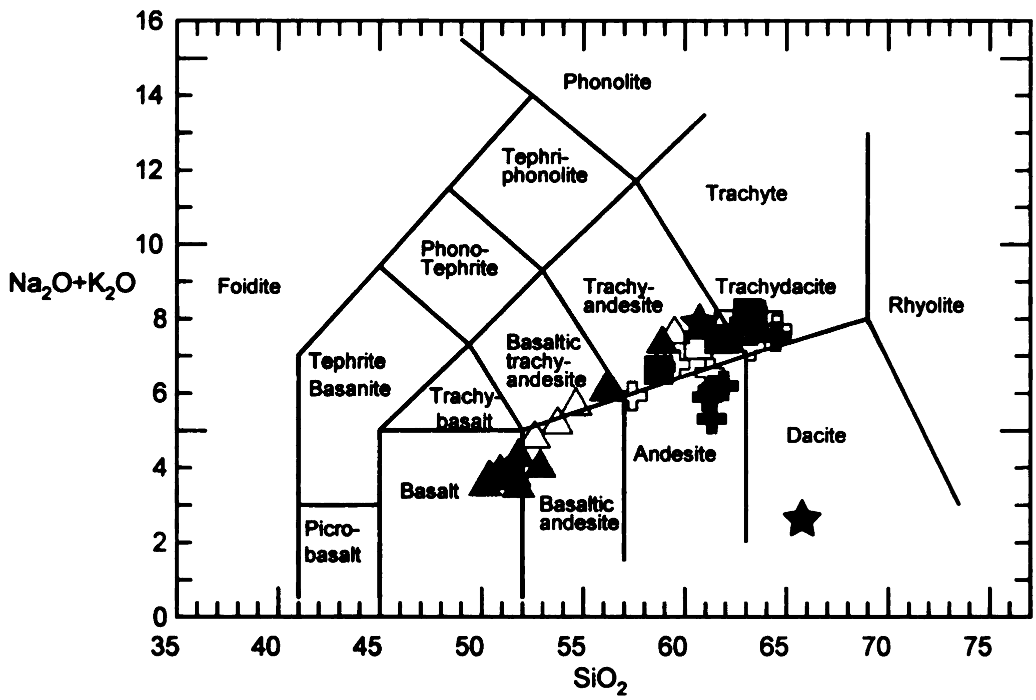

Figure 12. Total alkalis versus silica diagram. The samples plot in the basalt to the trachydacite field.

PIVS1 BH01 BH07 BH16

040303-1 040303-2 040303-3

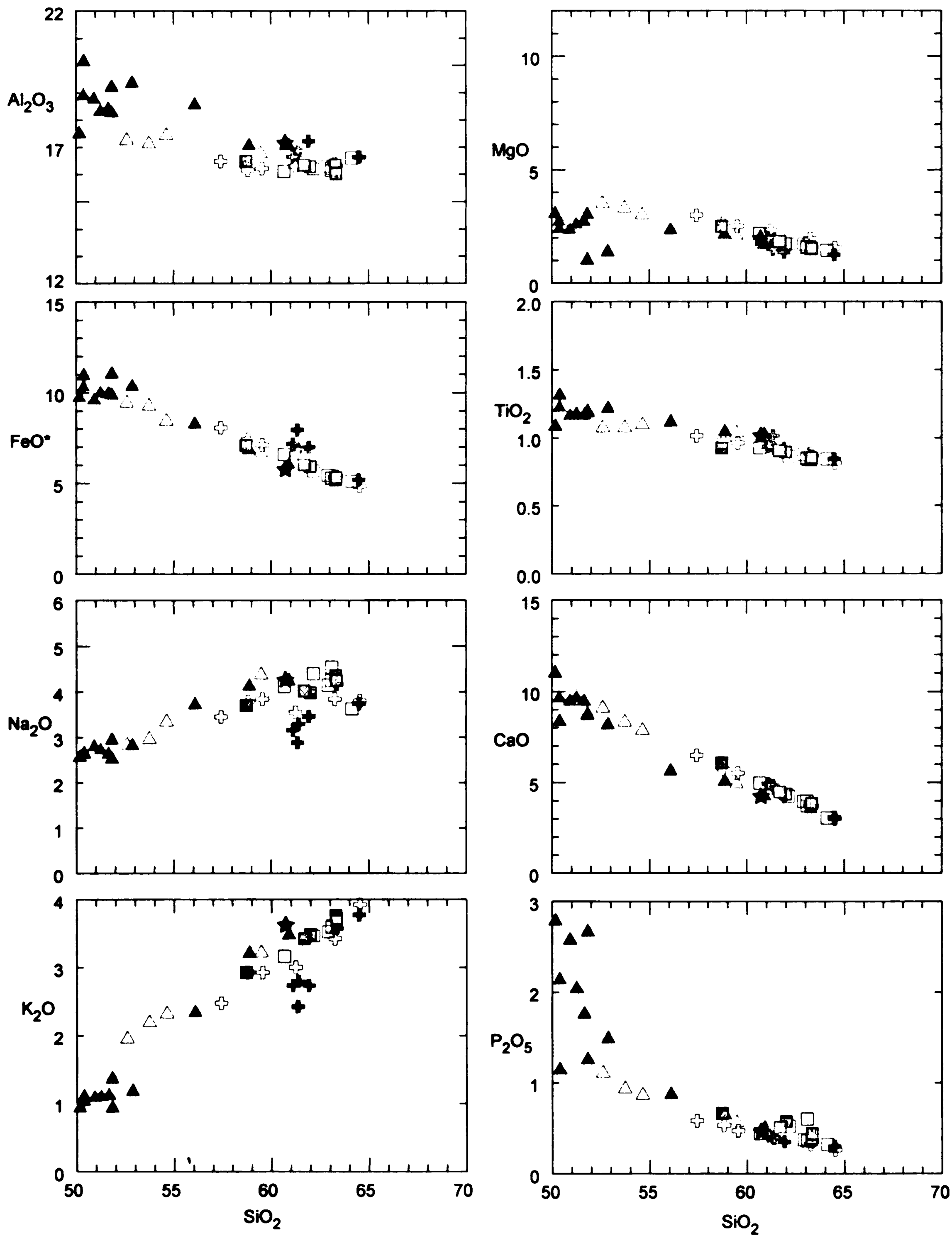

Figure 13. Major element variation with silica

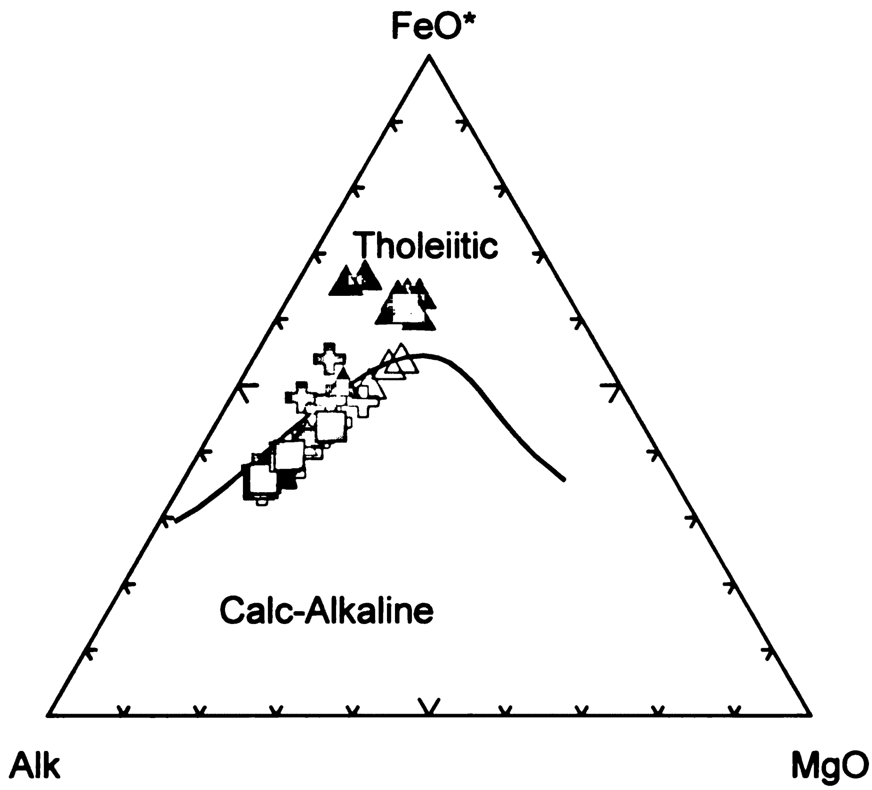

Figure 14. The pumices are enriched in Fe and in the AFM triangle, some plot in the tholeiitic field.

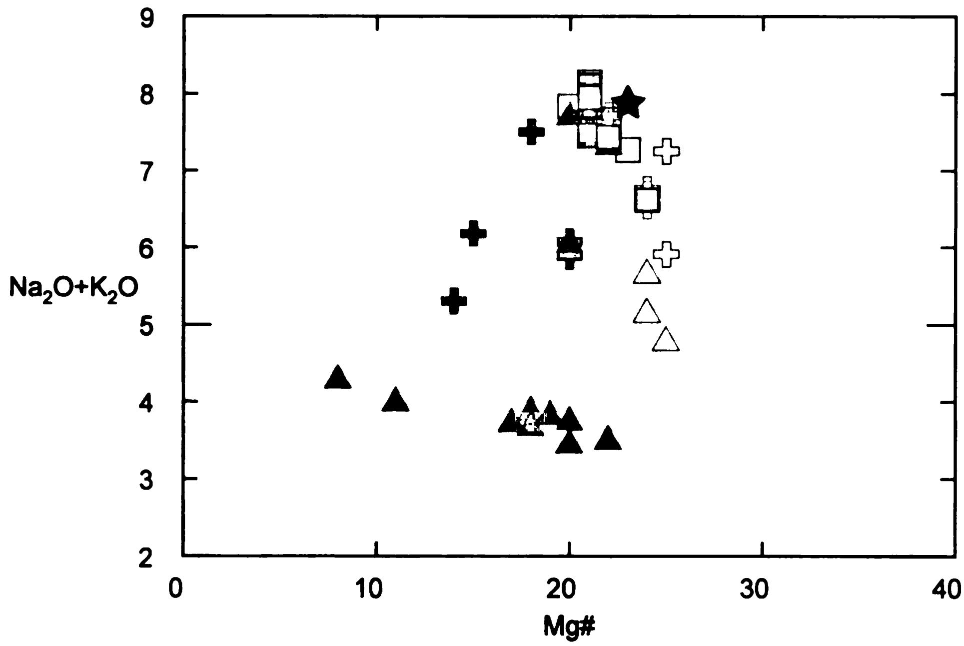

Figure 15. Total alkalis versus Mg#. A separate trend can be seen for the basaltic samples with high P_2O_5.

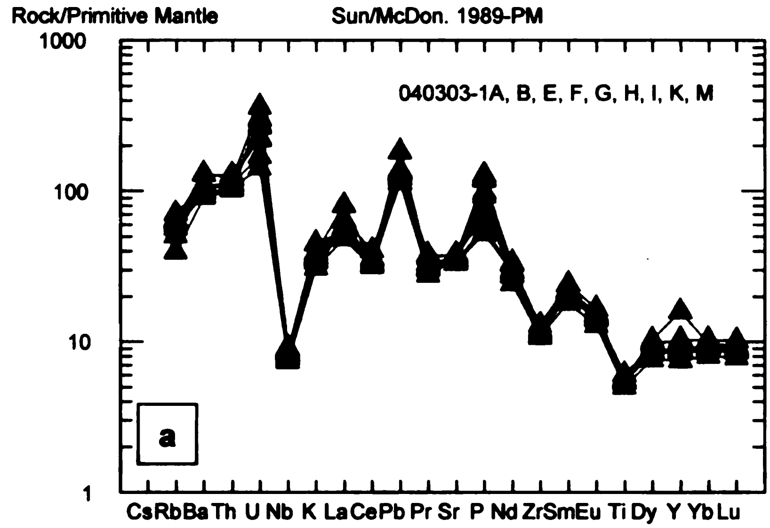

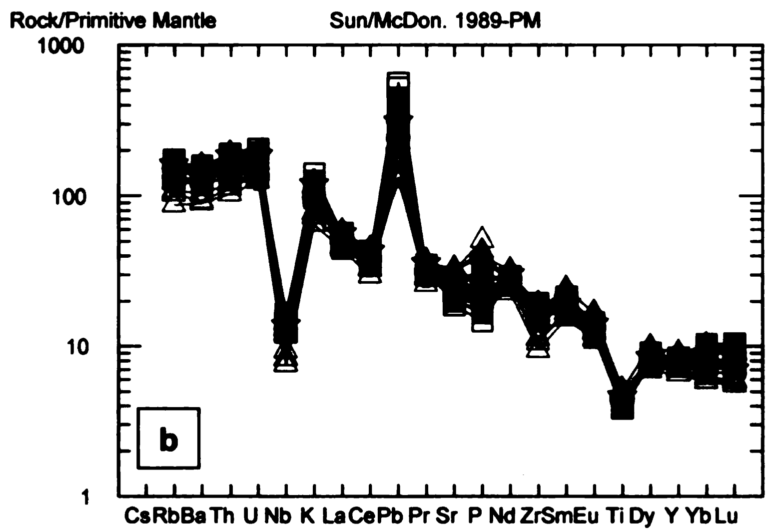

Figure 16. Trace element spider diagrams. Two groups were identified based on the spidergrams. One group consists of the basaltic high P_2O_5 pumices (a). Majority of the pumices are included in pattern b.

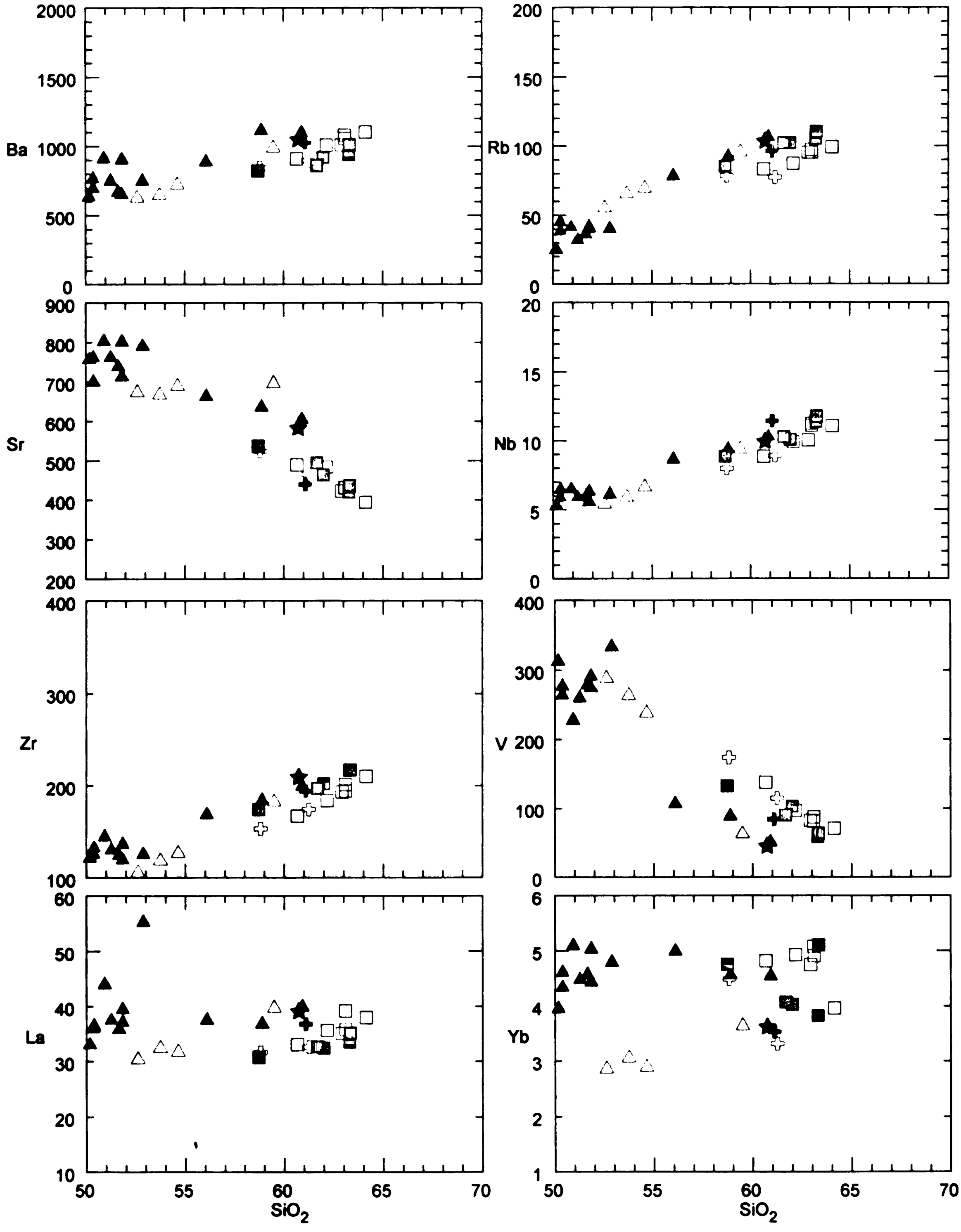

Figure 17. Trace element variation with silica. Note the higher and lower concentrations trends of Yb for the same value of silica.

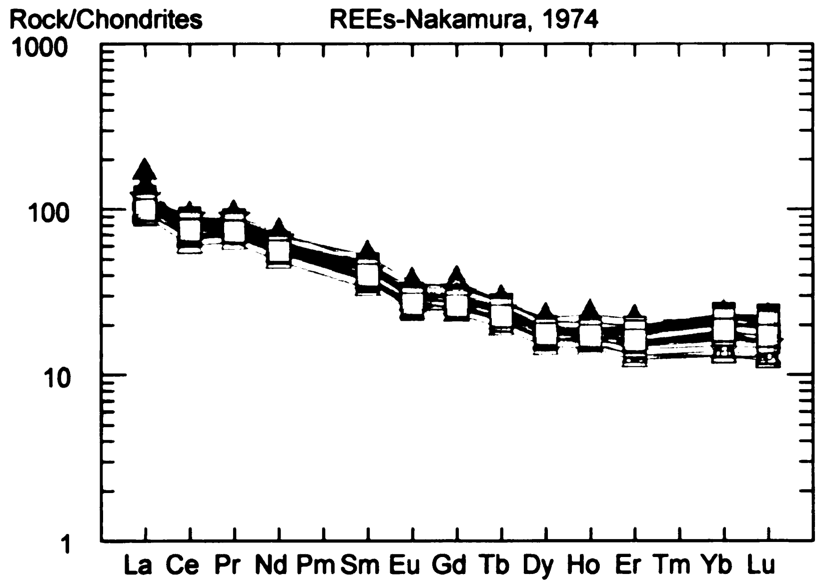

Figure 18. REE spidergrams. The samples include 50–64 wt. % SiO_2. A tight pattern is formed despite the range in silica, with decreasing concentration from light to heavy REE and a slightly concave upward trend towards the middle to heavy REE.

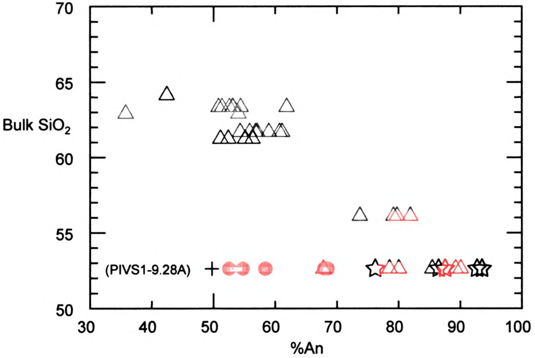

Figure 19. Generally the An content (values include rim and core analyses) of the plagioclases decrease in higher silica pumices. Plagioclases from enclaves found in pumice PIVS1-9.28A are included.

All pumice △ enclave 1 ● enclave 2 + enclave 3 ☆

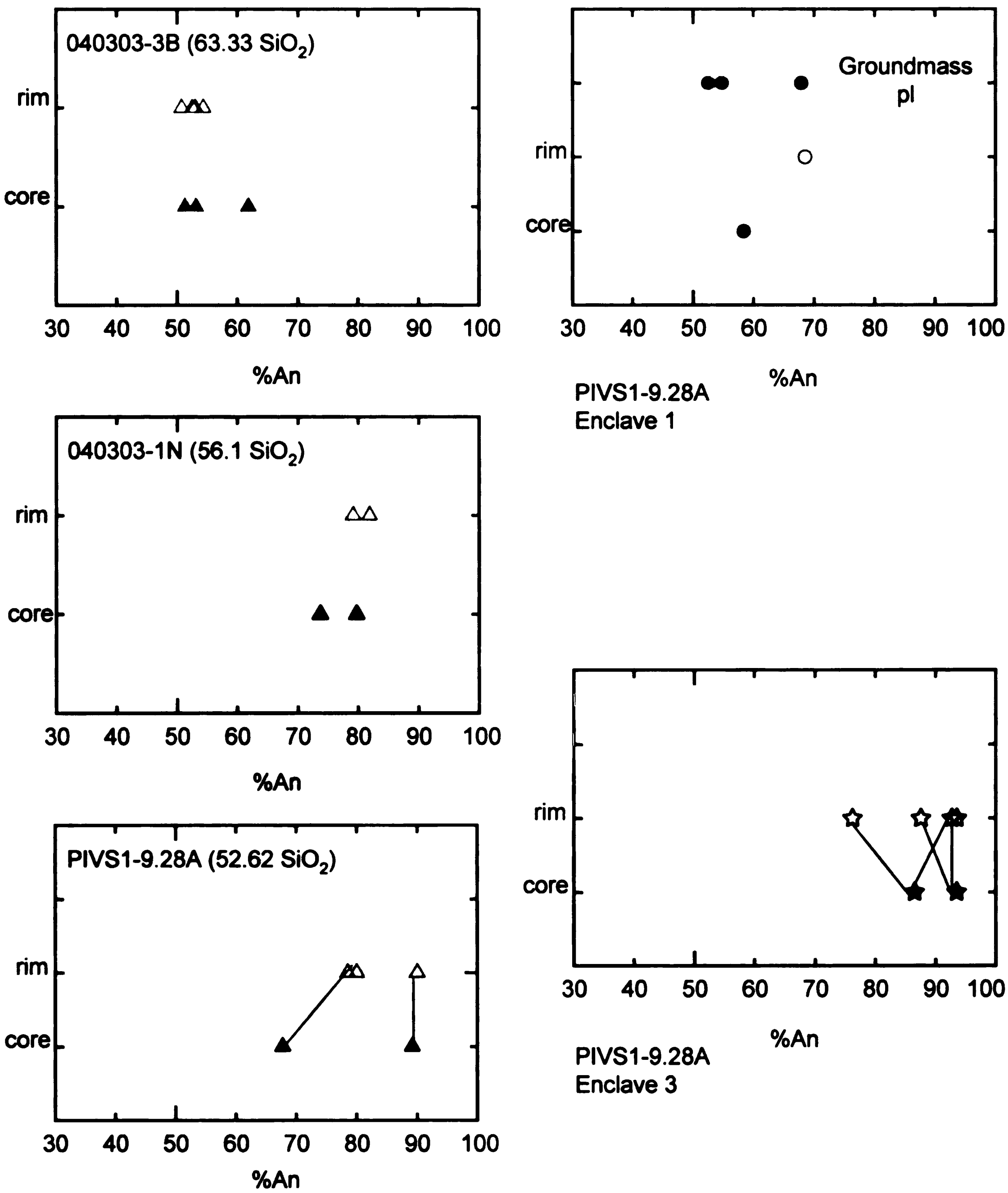

Figure 20. Plagioclase from different pumices, bulk silica content is indicated, showing the An values for the rim and core. Analysis on the enclaves is also included.

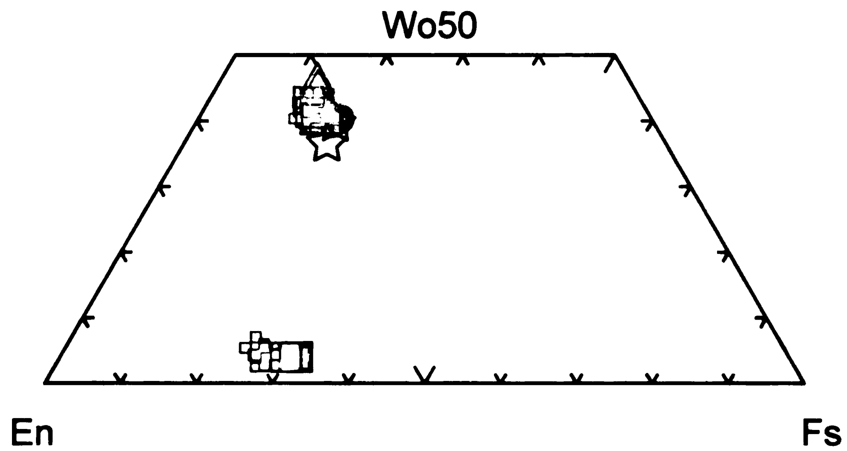

Figure 21. Classification of the pyroxenes in the samples. The pyroxenes plot in the diopside-augite and hypersthene fields.

BH07-03-P3 ✚ 040303-1N ▲ 040303-2C □ 040303-2F □ 040303-3B □

040303-3F □ PIVS1-9.28A △ enclave 1 ● enclave 3 ☆

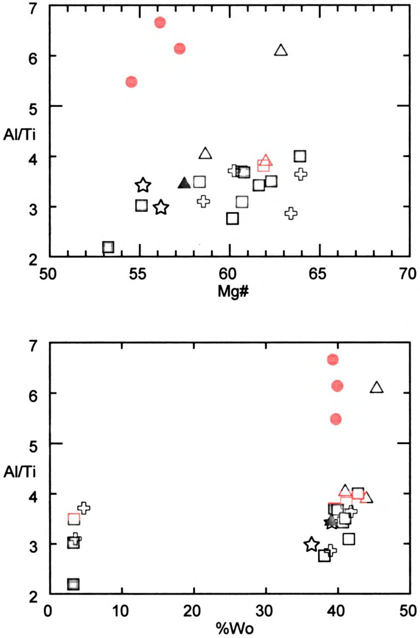

Figure 22. Two groups of pyroxenes can be seen in terms of Al/Ti ratios. Both groups have similar range of Mg # (Al/Ti vs. Mg#). The group with higher Al/Ti includes only clinopyroxenes (Al/Ti vs. Wo%).

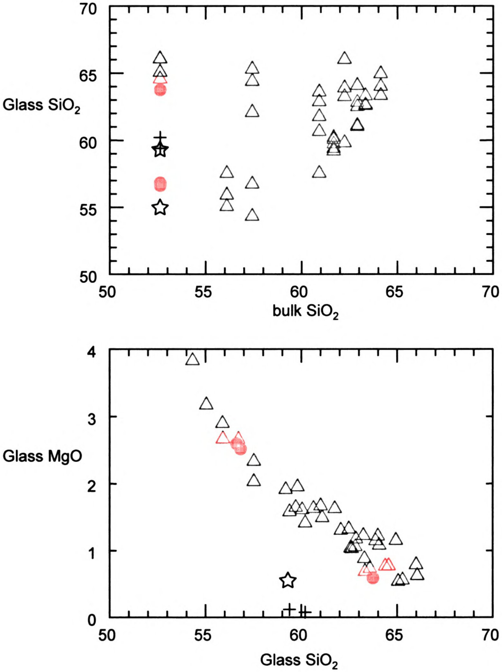

Figure 23. Variation in glass composition for the pumice fragments. The first plot shows groundmass glass silica against bulk silica. The second plot is MgO versus SiO_2 in glass, note that enclave 2 and 3 plot outside the trend.

Enclave 1 glass ● Enclave 2 glass + Enclave 3 glass ☆

PIVS1-9.28A pumice glass △ all other pumice glass △

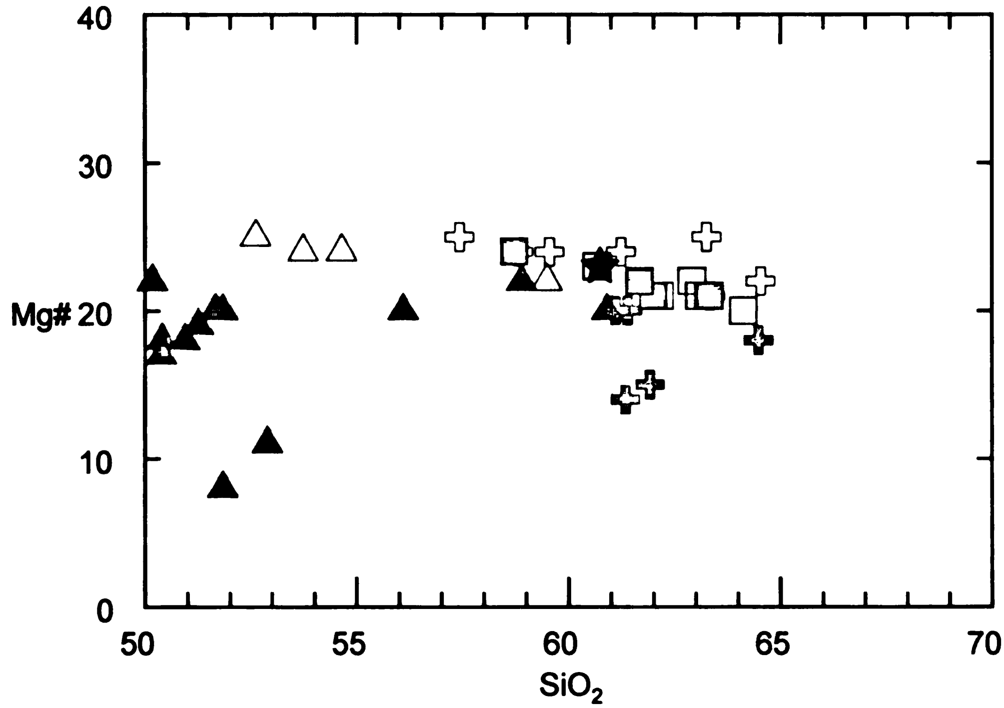

Figure 24. Almost constant Mg # for the upper Diliman tuff pumices as SiO_2 values increase, does not show a fractionation trend.

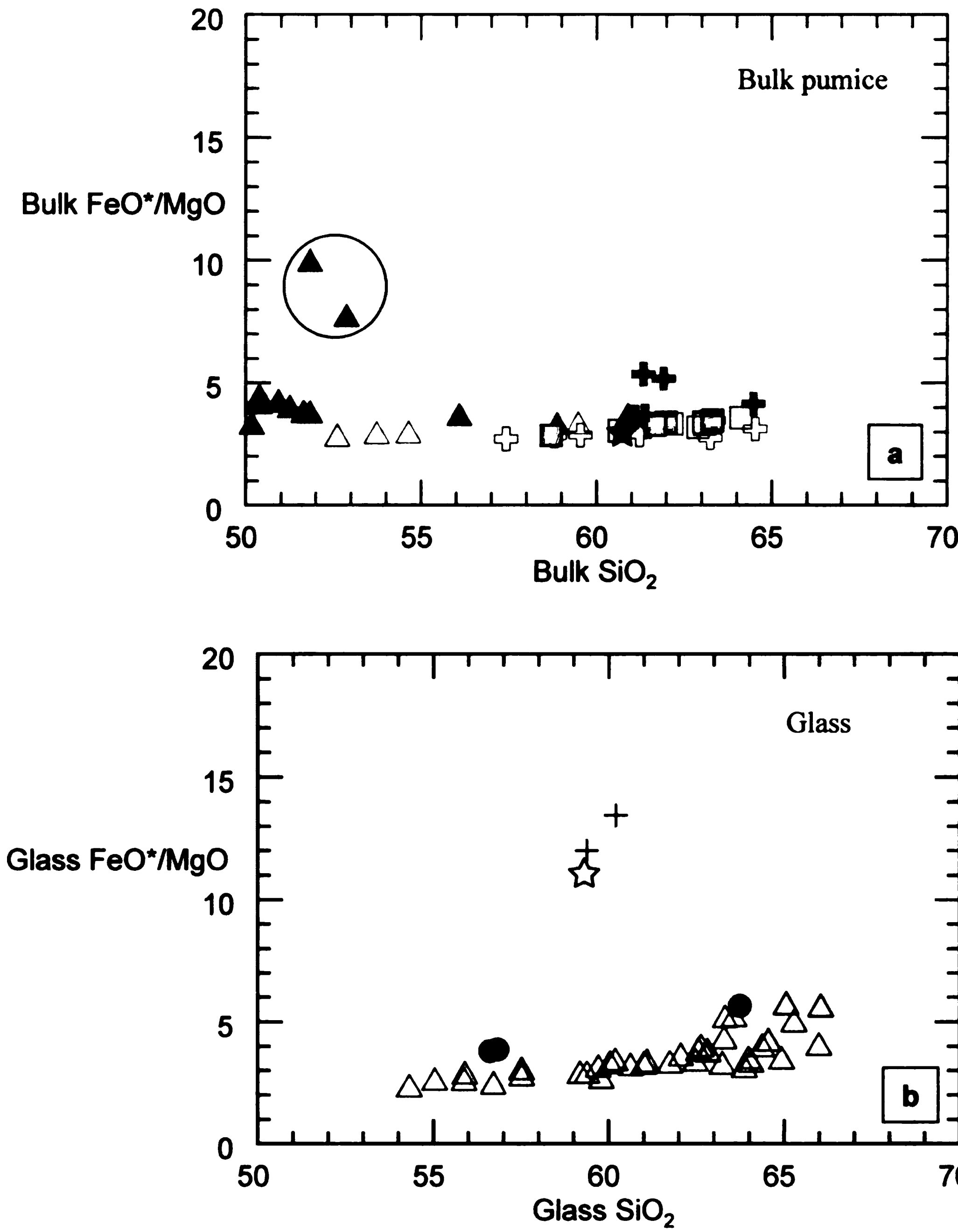

Figure 25.
a. Higher values of FeO*/MgO for bulk compositions of samples 040303-1I and 1F (circled).
b. Higher values of FeO*/MgO for glass compositions of enclave 2 and 3.

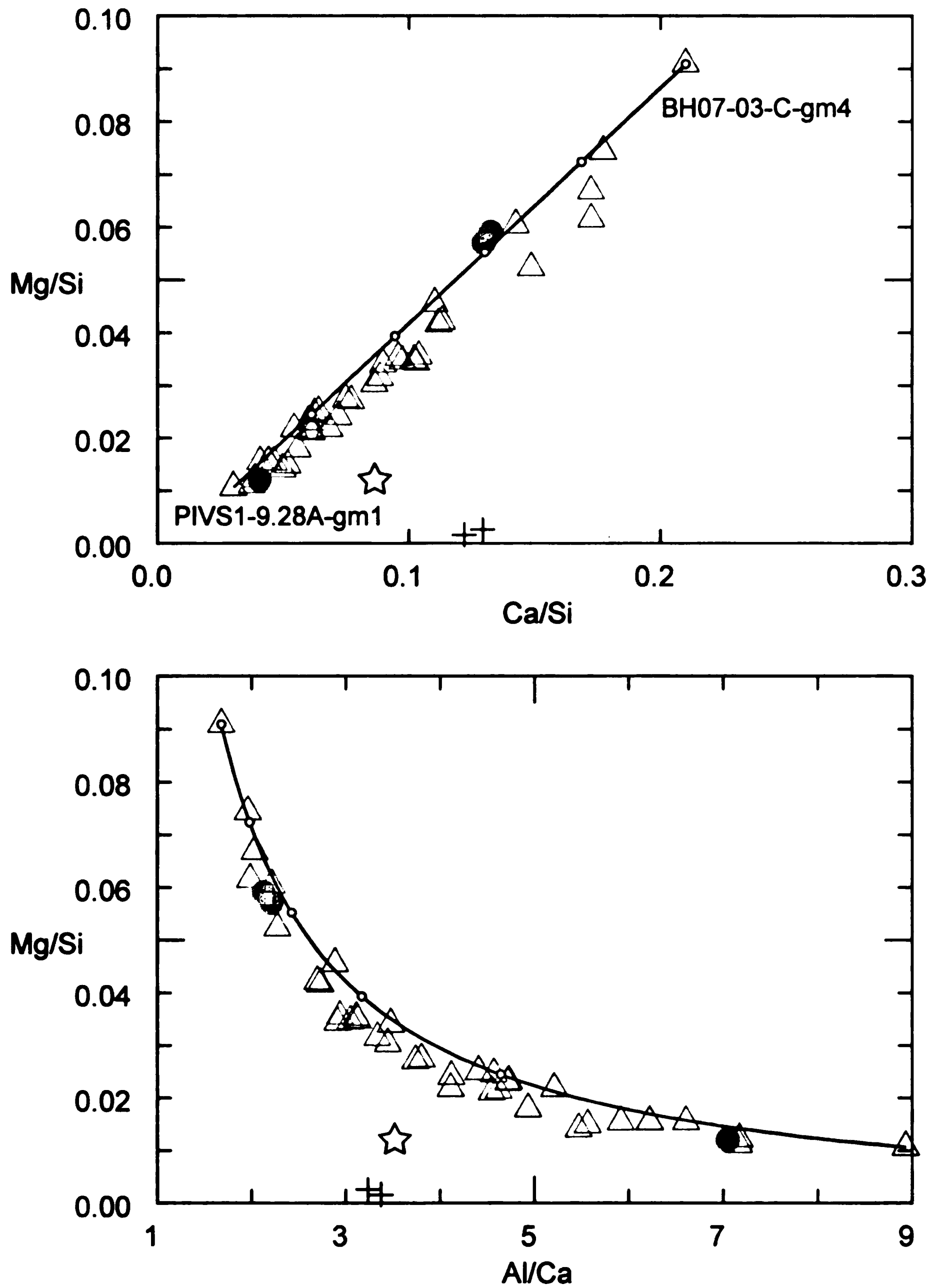

Figure 26. Mixing line for glass compositions. The end members cover the range of compositions but the fit of the mixing line is a little offset. Note glass from enclave 2 and enclave 3 plot outside the trend.

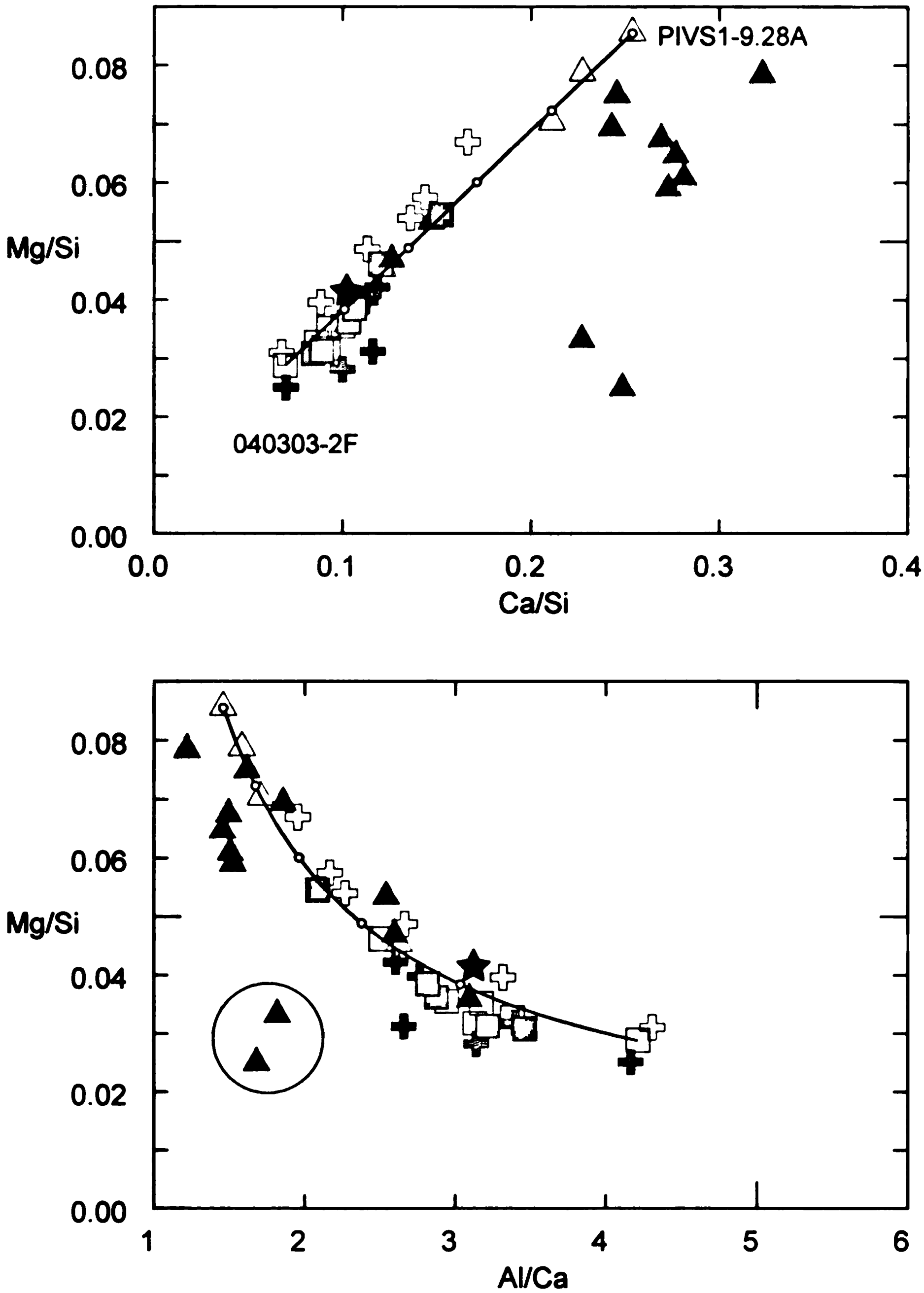

Figure 27. The same plot as figure 26 but using bulk pumice compositions. Note samples 040303-1I and 1F (circled) fall way off the trend.

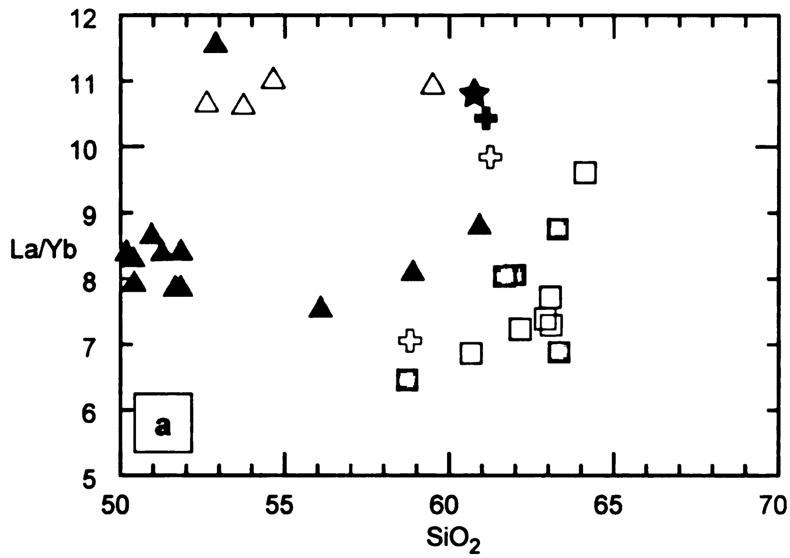

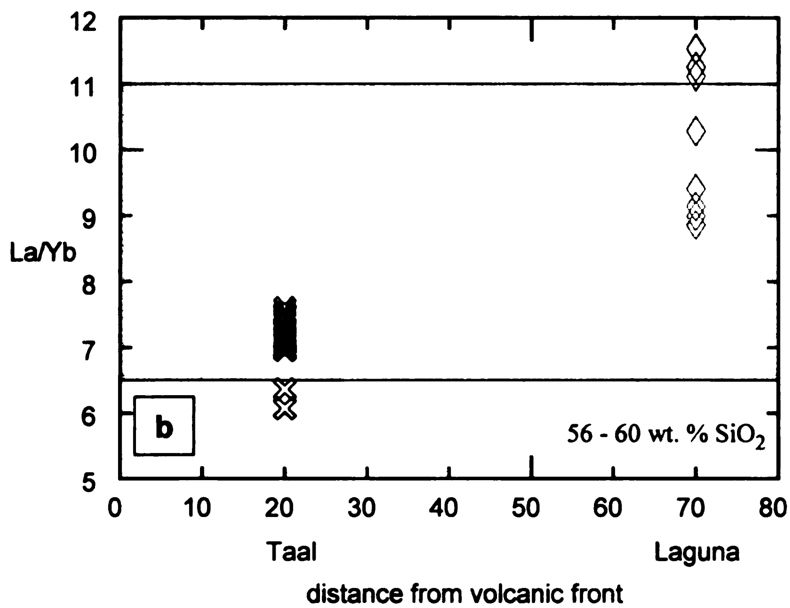

Figure 28.
a. La/Yb ratios for the upper Diliman Tuff show a scatter and a wide range from 6.5 to 11.5. (See Figure 12 for symbols).
b. La/Yb ratios for Taal and Laguna pumices in the andesitic range (56–60 wt.% SiO_2) plotted with respect to the distance of these centers from the volcanic front (Bataan arc). Location of the source vent for the upper Diliman Tuff is unknown, the values are represented by the shaded area. This graph shows higher values for Laguna pumices, which may be interpreted as lower degrees of melting; compared with Taal pumices. The upper Diliman Tuff is intermediate between the two.

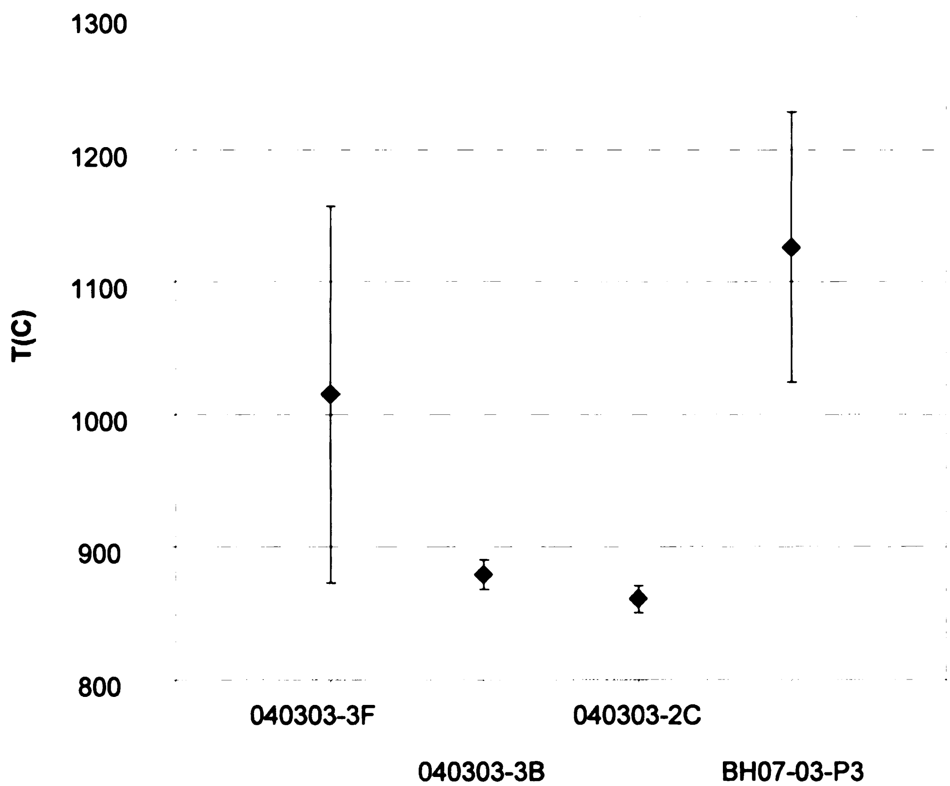

Figure 29. Geothermometry for coexisting orthopyroxene and clinopyroxene in pumice. Temperature estimates were done using QUILF (Andersen et al., 1993). Samples 040303-3B and 040303-2C have additional constraint from magnetite and give temperatures of 850 to 900°C with smaller uncertainty.

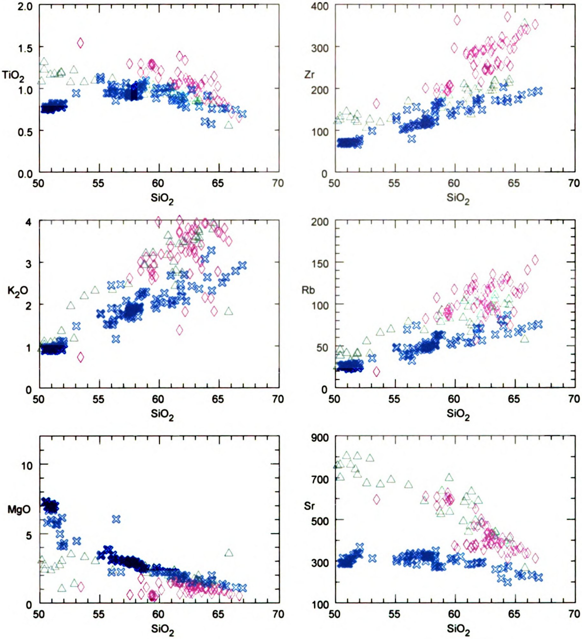

Figure 30. Comparison of major and trace element compositions of upper Dilimah Tuff and deposits from Taal and Laguna calderas. Sr values clearly distinguish Taal deposits. Differences between the upper Diliman Tuff and Laguna Tuff can be seen in MgO, TiO_2, and Zr. Taal data (Martinez, 1997; Listanco, 1993; Miklius et al., 1991); Laguna data (MSU data). Laguna ◇ Taal ✖ Upper Diliman Tuff △

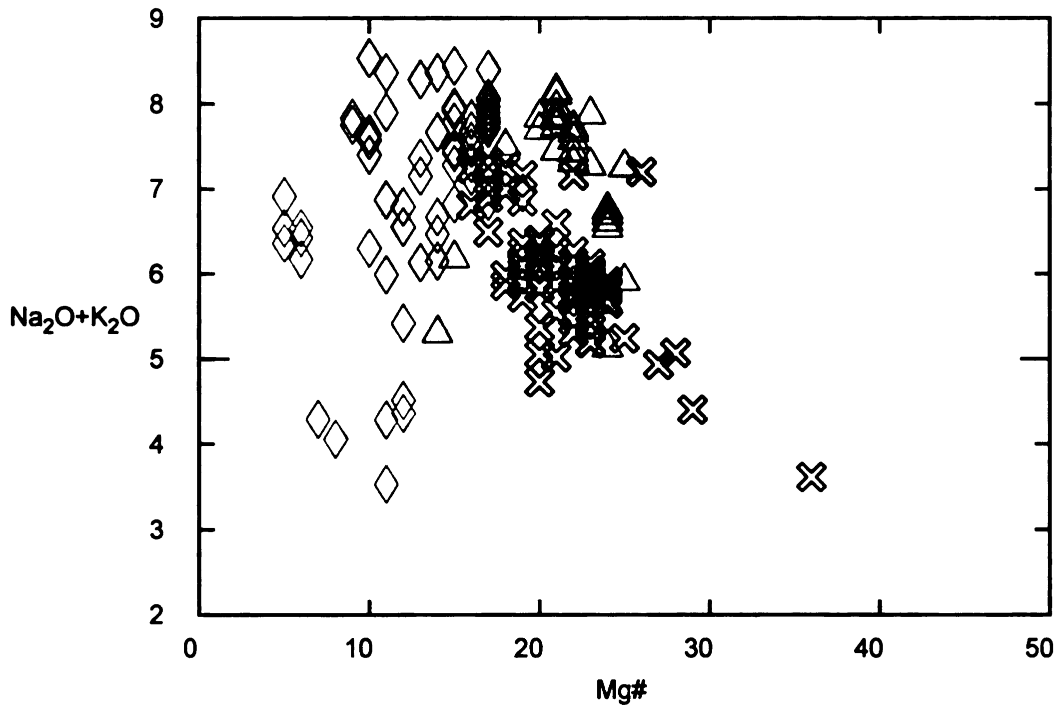

Figure 31. The clearest distinction between Laguna deposits and the upper Diliman Tuff is the Mg#. Upper Diliman and Taal pumices and lavas are more primitive than Laguna pumices.

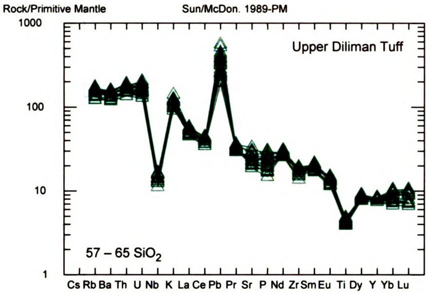

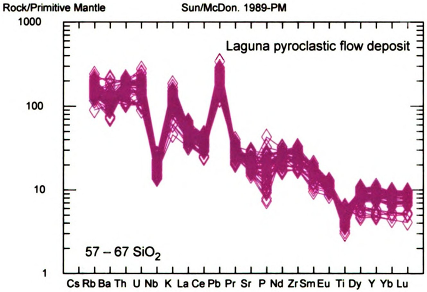

Figure 32. Trace element spidergrams show little difference between the upper Diliman Tuff and Laguna pumices.

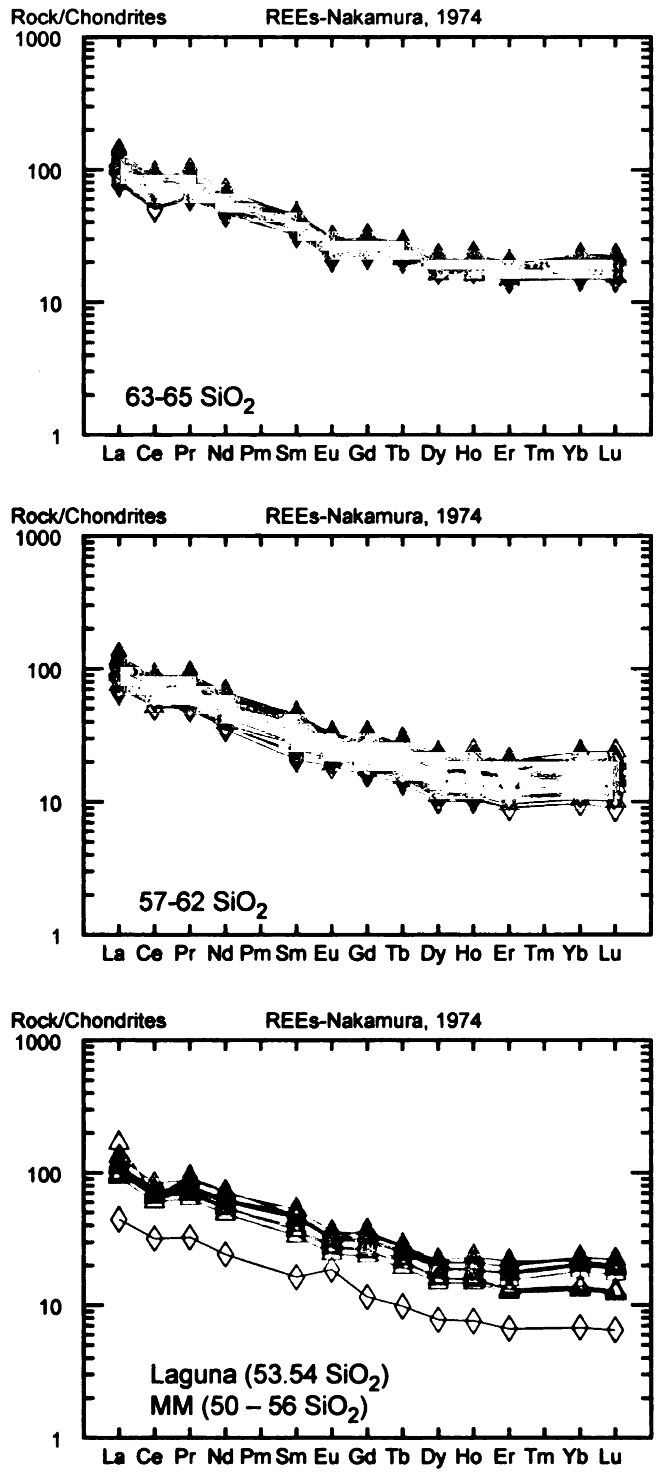

Figure 33. REE distribution for the upper Diliman Tuff shows a tight pattern from low silica to high silica pumices while Laguna REE concentrations have more variation.

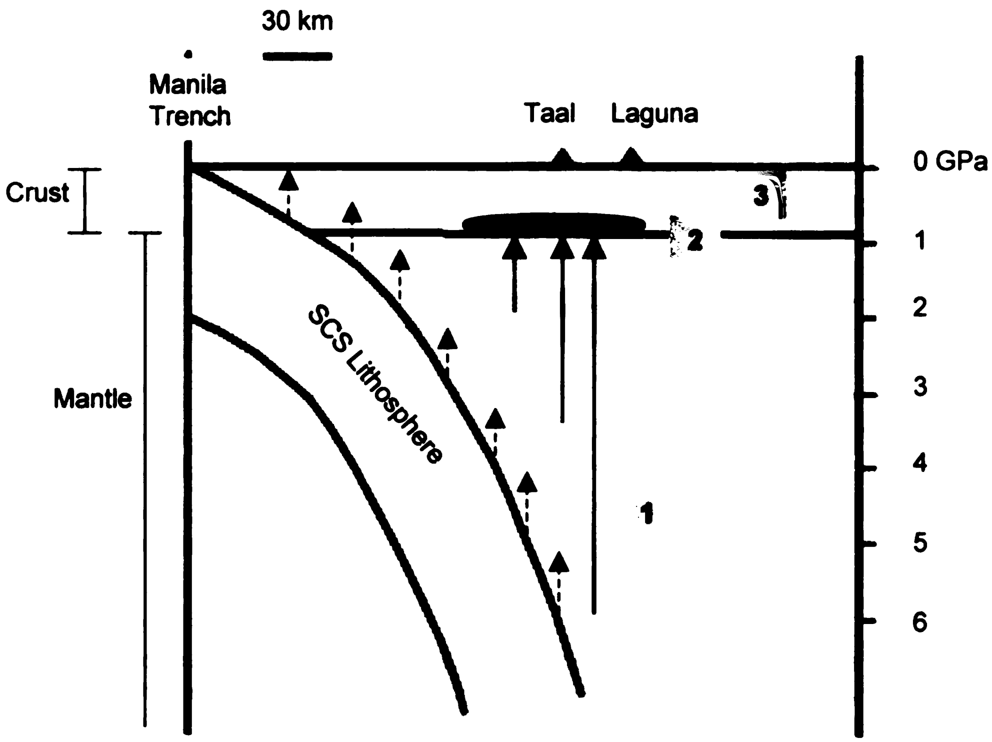

1: Fluids introduced by the subducted slab (represented by dashed blue arrows) metasomatise the mantle. Addition of fluids cause more melts to form and the melts rise (red arrows).

2: The melts stall beneath the crust and crystallize. They partially melt the surrounding crust comprised of previously emplaced arc magma

3: The melts rise, stall in mid-crust and partially melt surrounding crust (see figure 35).

Figure 34. Model for the evolution of the upper Diliman Tuff.

3a: Basaltic melts from deep in the upper mantle rise then stall at the lower crust. These melts rise again and pond at the mid-crust and melt surrounding rocks.

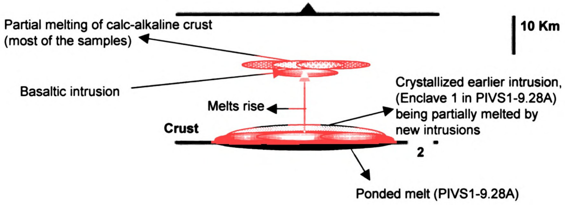

3b: New basaltic melts (tholeiitic) rise and intrude the previous intrusion. The different melts are then erupted as a chemically variable pyroclastic flow deposit.

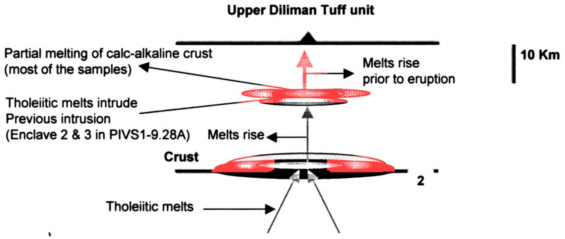

Figure 35. Model for the evolution of the upper Diliman Tuff (continued).

REFERENCES

Alvir, A. (1929). A geological study of the Angat-Novaliches region. Philippine J. of Science: 40, 359-419.

Andersen, D, Lindsley, D. and Davidson, P. (1993). QUILF: A pascal program to assess equilibria among Fe-Mg-Mn-Ti oxides, pyroxenes, olivine, and quartz. Computers and Geosciences: 19, 1333-1350.

Annen, C. and Sparks, R. (2002). Effects of repetitive emplacement of basaltic intrusions on thermal evolution and melt generation in the crust. Earth and Planetary Science Letters: 203, 937-955.

Arcilla, C. (1991). Lithology, age and structure of the angat ophiolite Luzon, Philippine Islands. MS Thesis. University of Illinois at Chicago.

Besana, G, Shibutani, T, Hirano, N, Ando, M, Bautista, B, Narag, I. and Punongbayan, R. (1995). The shear wave velocity structure of the crust and uppermost mantle beneath Tagaytay, Philippines inferred from receiver function analysis. Geophysical Research Letters: 22, 3143-3146.

Cardwell, R, Isacks, B. and Karig, D. (1980). The spatial distribution of earthquakes, focal mechanism solutions and subducted lithosphere in the Philippines and Northern Indonesia regions. In DE Hayes (Editor), <u>The tectonic and geologic evolution of Southeast Asian seas and islands.</u> AGU Geophysical Monograph: 23, 1-35.

Cas, R. and Wright, J. (1993). <u>Volcanic successions: modern and ancient</u>. London: Chapman and Hall.

Castillo, P. and Newhall, C. (2004). Geochemical constraints on possible subduction components in lavas of Mayon and Taal volcanoes, Southern Luzon, Philippines. Journal of Petrology: 45, 1089-1108.

Catane, S. and Arpa, M. (1998). Large-scale eruptions of Laguna caldera: contributions to the accretion and other geomorphic developments of Metro Manila and adjacent provinces. PHIVOLCS internal report.

Corby, G. (1951). <u>Geology and oil possibilities of the Philippines</u>. Manila: Dept. Agr. Nat. Res., Phil. Tech. Bull., 21.

De Boer, J, Odom, L, Ragland, P, Snider, F. and Tilford, N. (1980). The Bataan orogene: eastward subduction, tectonic rotations, and volcanism in the Western Pacific. Tectonophysics: 67, 251-282.

Defant, M, De Boer, J. and Oles, D. (1988). The western central Luzon volcanic arc, The Philippines: two arcs divided by rifting? Tectonophysics: 145, 305-317.

Defant, M, Jacques, D, Maury, R, De Boer, J. and Joron, J-L. (1989). Geochemistry and tectonic setting of the Luzon arc, Philippines. Geol Soc Am Bull: 101, 663-672.

Dungan, M. (2005). Partial melting at the Earth's surface: implications for assimilation rates and mechanisms in subvolcanic intrusions. Journal of Volcanology and Geothermal Research: 140, 193-203.

Fisher, R. and Schmincke, H. (1984). Pyroclastic Rocks. Springer.

Flood, T, Vogel, T, Arpa, M, Patino, L, Catane, S. and Arcilla, C. (2004). Silicic magmas erupted from the Laguna de Bay Caldera, Macolod Corridor, Luzon, Philippines: geochemistry and origin. AGU Fall Meeting.

Forster, H, Oles, D, Knittel, U, Defant, M. and Torres, R. (1990). The Macolod Corridor: A rift crossing the Philippine island arc. Tectonophysics: 183, 265-271.

Galgana, G, Hamburger, M, Torres, R, McCaffrey, R. and Chen, Q. (2004). Crustal deformation of Luzon Island, Philippines from GPS-based geodynamic models and structural analyses of satellite imagery. AGU Fall Meeting.

Gervasio, F. (1968). The geology, structures and landscape development of Manila and suburbs. Philippine Geologist: 22, 178-192.

Giggenbach, W. (1992). Isotopic shifts in waters from geothermal and volcanic systems along convergent plate boundaries and their origin. Earth and Planetary Science Letters: 113, 495-510.

Gonzales, B, Ocampo, V. and Espiritu, E. (1971). Geology of Southwestern Nueva Ecija and Eastern Bulacan provinces, Luzon Central Valley. J. Geol. Soc. Philippines: 25, 3-41.

Grove, T, Elkins-Tanton, L, Parman, S, Chatterjee, N, Muntener, O. and Gaetani, G. (2003). Fractional crystallization and mantle-melting controls on calc-alkaline differentiation trends. Contrib Mineral petrol: 145, 515-533.

Hall, R, Fuller, M, Ali, J. and Anderson, C. (1995). The Philippine Sea Plate: magnetism and reconstructions. In B Taylor and J Natland (Editors), Active margins and marginal basins of the Western Pacific. AGU Geophysical Monograph: 88, 371-401.

Hamburger, M, Cardwell, R. and Isacks, B. (1983). Seismotectonics of the northern Philippine Island Arc. In Hayes DE (ed). The tectonic and geologic evolution of Southeast Asian Seas and Islands, Part2. Am Geophys. Union Monogr.: 27, 1 – 22.

Hannah, R, Vogel, T, Patino, L, Alvarado, G, Perez, W. and Smith, D. (2002). Origin of silicic volcanic rocks in Central Costa Rica: A study of a chemically variable ash-flow sheet in the Tiribi Tuff. Bulletin of Volcanology: 64, 117-133.

Hayes, D. and Lewis, S. (1984). A geophysical study of the Manila Trench, Luzon, Philippines 1. Crustal structure, gravity, and regional tectonic evolution. Journal of Geophysical Research: 89, 9171-9195.

Hildreth, W. and Fierstein, J. (2000). Katmai volcanic cluster and the great eruption of 1912. GSA Bulletin: 112, 1594-1620.

Irving, E. (1947). Geomorphological implications of the Marikina drainage pattern Rizal province, Luzon, Philippine Islands. The Philippine Geologist: 10, 1-12.

Karig, D. (1973). Plate convergence between the Philippines and the Ryuku Islands. Maine Geology: 14, 153-168.

Knittel, U. and Defant, M. (1988). Sr isotopic and trace element variations in Oligocene to recent igneous rocks from the Philippine island arc: evidence for Recent enrichment in the sub-Philippine mantle. Earth and Planetary Science Letters: 87, 87-99.

Knittel, U, Defant, M. and Raczek, I. (1988). Recent enrichment in the source region of arc magmas from Luzon Island, Philippines: Sr and Nd isotopic evidence. Geology: 16, 73-76.

Listanco, E. (1993). Space-time patterns in the geologic and magmatic evolution of calderas: a case study at Taal Volcano, Philippines. Ph.D. Thesis, University of Tokyo.

Martinez, M. (1997). Stratigraphy and geochemistry of Taal Caldera scoria pyroclastic flow deposit, Philippines. M.S. Thesis, Arizona State University.

McCabe, R, Alamasco, J. and Yumul, G. (1985). Terranes of the Central Philippines. In DH Howell (Editor), Tectonostratigraphic terrains of Circum-Pacific Region. Circum-Pacific energy and mineral resources. Earth Science: 1, 421-436.

McGovern, P. and Schubert, G. (1989). Thermal evolution of the Earth: effects of volatile exchange between atmosphere and interior. Earth and Planetary Science Letters: 96, 27-37.

Miklius, A, Flower, M, Huifsmans, J, Mukasa, S. and Castillo, P. (1991). Geochemistry of lavas from Taal Volcano, Southwestern Luzon, Philippines: Evidence for multiple magma supply systems and mantle source heterogeneity. Journal of Petrology: 32, 593-627.

Mukasa, S, Flower, M. and Miklius, A. (1994). The Nd-, Sr- and Pb-isotopic character of lavas from Taal, Laguna de Bay and Arayat volcanoes, southwestern Luzon, Philippines: implications for arc magma petrogenesis. Tectonophysics: 235, 205-221.

Obile, E. Jr. (1995). Pyroclastic flow deposit of the Laguna Formation at Sitio Canlibot and Sitio Cubanbaan. Bagumbayan, Teresa, Rizal. M.S. Thesis, University of the Philippines, Diliman.

Ocampo, V. and Martin, S. (1967). Report on the geology and section measurements in southern Luzon Central Valley, Philippines. Unpubl. Report. Bu. Of Mines, petroleum division, Manila.

Oles, D, Knittel, U, Forster, H, Torres, R, Wolfe, J. and Bellon, H. (1995). Basaltic volcanism associated with extensional tectonics in the southern part of the Luzon Island Arc, The Philippines: Part I. Tectonic setting and volcanological evolution. Unpublished report, Institute of Mineralogy, RWTH Aachen, Germany and Philippine Institute of Volcanology and Seismology, Philippines.

Ozawa, A, Tagami, T, Listanco, E, Arpa, M. and Sudo, M. (2004). Initiation and propagation of subduction along the Philippine Trench: evidence from the temporal and spatial distribution of volcanoes. Journal of Asian Earth Sciences: 23, 105-111.

Pautot, G. and Rangin, C. (1989). Subduction of the South China Sea axial ridge below Luzon (Philippines). Earth and Planetary Science Letters: 92, 57-69.

Peacock, S. (1990). Fluid processes in subduction zones. Science: 248, 329-337.

Pilet, S, Hernandez, J. and Villemant, B. (2002). Evidence for high silicic melt circulation and metasomatic events in the mantle beneath alkaline provinces: the Na-Fe-augitic green-core pyroxenes in the Tertiary alkali basalts of the Cantal massif (French Massif Central). Mineralogy and Petrology: 76, 39-62.

Pubellier, M, Garcia, F, Loevenbruck, A. and Chorowicz, J. (2000). Recent deformation at the junction between the North Luzon block and the Central Philippines from ERS-1 Images. The Island Arc: 9, 598-610.

Rangin, C, Stephan, J. and Muller, C. (1985). Middle Oligocene oceanic crust of South China Sea jammed into the Mindoro collision zone (Philippines). Geology: 13, 425-428.

Rangin, C, Silver, E. and Tamaki, K. (1995). Closure of the Western Pacific marginal basins: rupture of the oceanic crust and the emplacement of ophiolites. In B Taylor and J Natland (Editors), Active margins and marginal basins of the Western Pacific. AGU Geophysical Monograph: 88, 405-415.

Rollinson, H. (1993). Using geochemical data: evaluation, presentation, interpretation. NY: Longman.

Rudnick, R. and Fountain, D. (1995). Nature and composition of the continental crust: A lower crustal perspective. Reviews of Geophysics: 33, 267-309.

Saxena, S. (1976). Two-pyroxene geothermometer: a model with an approximate solution. American Mineralogist: 61, 643-652.

Smith, G. (2000). Essential volcanology for the field study of continental volcanic rocks: An informal manual for "Field Studies in Volcanology". University of New Mexico.

Smith, I, Worthington, T, Stewart, R, Price, R. and Gamble, J. (2003). Felsic volcanism in the Kermadec arc, SW Pacific: crustal recycling in an oceanic setting. In Larter, D. and Leat, P. (editors). Intra-oceanic subduction systems: tectonic and magmatic processs. Geol Soc, London, Special Publications: 219, 99-118.

Smith, R. (1979). Ash-flow magmatism, in Chapin CE, and Elston WE, eds., Ash-flow tuffs. Geological Society of America Special Paper 180.

Smith, W. (1924). Geology and mineral resources of the Philippine Islands. Manila: Bureau of Science Publication.

Tatsumi, Y. (1989). Migration of fluid phases and genesis of basalt magmas in subduction zones. Journal of Geophysical Research: 94, 4697-4707.

Tatsumi, Y. and Eggins, S. (1995). Subduction zone magmatism. Blackwell Science. p. 109.

Taylor, B. and Hayes, D. (1983). Origin and history of the South China Sea basin. In Hayes, D. (editor). The Tectonic and Geologic Evolution of Southeast Asian Seas and Islands. Am. Geophys. Union, Geophys. Monogr.: 23, 89-104.

Teves, J. and Gonzales, M. (1950). The geology of the university site – Balara area, Quezon City. The Philippine Geologist: 4, 1 – 10.

Thompson, R. (1974). Some high-pressure pyroxenes. Mineral Mag: 39, 768-787.

Torres, R, Miklius, A. and Rimando, R. (1986). Accomplishment report of the geological survey of Morong Peninsula and Talim Island. PHIVOLCS internal report.

Vogel, T, Patino, L, Alvarado, G. and Gans, P. (2004). Silicic ignimbrites within the Costa Rican volcanic front: evidence for the formation of continental crust. Earth and Planetary Science Letters: 226, 149-159.

Winter, J. (2001). An introduction to igneous and metamorphic petrology. NJ: Prentice Hall. p. 299.

Wolfe, J. and Self, S. (1983). Structural lineaments and Neogene volcanism in southwestern Luzon. In DE Hayes (Editor), The Tectonic and Geologic Evolution of Southeast Asian Seas and Islands, Part 2. Am. Geophys. Union Geophys. Monogr.: 27, 157-172.

Zanoria, E. (1988). The depositional and volcanological origin of the Diliman volcaniclastic formation, Southwestern Luzon, Philippines. Thesis. University of Illinois at Chicago.